Determination of the fracture envelope of an adhesive joint as a function moisture

Tânia Alexandra Ferreira Rodrigues

A dissertation submitted for Master's Degree in Mechanical Engineering

Supervisor: Prof. Lucas F.M. da Silva

Co- supervisor: Dr. Filipe Chaves

U.PORTO

FEUP FACULDADE DE ENGENHARIA
UNIVERSIDADE DO PORTO

July 2015

To my family

Abstract

Adhesively joints are increasingly being used in aerospace, automotive and maritime industries. The use of this type of joining provides some advantages such as reduction in weight and cost. However, adhesive joints in transportation industry may be exposed to aggressive environments such as high humidity during their service life. A particular issue with the reliability of adhesive joints is the presence of cracks and flaws. Fracture mechanics tests for adhesive joints provide relevant mechanical properties to determine the adhesive toughness and play an important role in design process.

This research aims to determine the fracture toughness of aluminum/adhesive/aluminum joints under pure mode I, pure mode II and mixed mode loadings. The fracture characterization of adhesively joints was performed when these specimens were submitted to mixed mode loadings and pure modes (shear and opening). The experimental tests Double Cantilever Beam (DCB) and End-Notched Flexure (ENF) were also done in order to assess the fracture toughness in pure modes I and II, respectively. A mixed mode apparatus was used to perform the mixed mode tests from pure mode I to near mode II. Test for dry and wet condition were performed with the main purpose to predict the influence of humidity in the toughness properties. The adhesive characterized was a ductile epoxy adhesive, Nagase Chemtex® XNR 6852E-2.

The diffusion coefficient was measured and the water uptake behavior was studied for a temperature of 50 ºC. Finite element analysis (FEA) was carried out to predict the moisture content in the adhesive layer, using ABAQUS®.

The influence of water in the behavior of the adhesive joint (DCB) was verified by changes in the values of the fracture mechanics properties. The load necessary to initiate a crack propagation is lower for aged adhesive joints when compared with dry adhesive joints for pure modes and different mixed mode ratios.

Resumo

As ligações adesivas são cada vez mais utilizadas na indústria aeroespacial, automóvel e naval. A utilização deste tipo de ligação fornece algumas vantagens, tais como redução do peso e do custo. Contudo, na indústria dos transportes, estas ligações podem ser expostas a ambientes agressivos, tais como ambientes com elevada humidade durante a sua vida útil. Uma questão particular é a fiabilidade das juntas adesivas na presença de fendas e falhas. Os ensaios de mecânica da fratura para juntas adesivas proporcionam propriedades mecânicas relevantes, de forma a determinar a resistência adesiva e desempenham um papel importante no processo de design de juntas.

Esta pesquisa tem como objetivo determinar a tenacidade à fratura de juntas de alumínio / adesivo / alumínio em modo puro I, II e modo misto. A caracterização à fratura de juntas adesivas foi realizada quando estas estavam submetidas a cargas de modo misto e modos puros (corte e abertura). Os ensaios Double Cantilever Beam (DCB) e End-Notched Flexure (ENF) foram realizados para avaliar a resistência à fratura em modos puros I e II, respetivamente. Um dispositivo foi usado para realizar os ensaios de modo misto, de modo I puro, chegando até perto de modo II. Foram feitos ensaios com provetes com e sem humidade de forma a prever a influência da mesma na tenacidade. O adesivo caraterizado foi um epóxido dúctil, Nagase Chemtex® XNR 6852E-2.

O coeficiente de difusão foi medido e o comportamento do adesivo a absorver água foi estudado para uma temperatura de 50ºC. Foi feita uma análise com elementos finitos, recorrendo ao software ABAQUS®, para prever a distribuição de humidade pela camada adesiva.

A influência da água no comportamento da junta adesiva (DCB) foi verificada pela alteração nos valores da tenacidade à fratura. A força necessária para a propagação estável da fenda é menor em juntas adesivas sujeitas a envelhecimento com água quando comparado com juntas em meios secos para modos puros e para diferentes combinações de modos.

Acknowledgements

I would like to express my sincere gratitude and appreciation to my supervisor, Professor Lucas Filipe Martins da Silva, for providing me with the continuous guidance and for giving me the opportunity to work under his supervision.

I would also like to acknowledge Dr. Filipe Chaves for his invaluable help and patience during the long hours developing my master thesis.

All the personnel in the AdFEUP, especially Dr. Ricardo Carbas, Eng. Ana Queirós and Eng. Rosa Paiva for the help and advice while developing this thesis. A special thanks to Joana, Daniel and Rodrigo for the friendship and for being always by my side during this semester.

And finally, all my family and friends for the support when I needed the most.

Contents

List of acronyms and symbols

Acronyms

4ENF	Four-point End Notched Flexure
ADCB	Asymmetric Double Cantilever Beam
CBBM	Compliance-Based beam method
CZM	Cohesive Zone Model
DCB	Double cantilever beam
ELS	End Loaded Split
ENF	End notched flexure
FEA	Finite Element Analysis
FPZ	Fracture process zone
MMB	Mixed Mode Bending
R-Curve	Resistance Curve

Symbols

a	crack length
a_0	initial crack growth
a_{eq}	equivalent crack length
B	width of the adherend
C	compliance
C_0	initial specimen compliance
Δa	crack growth
F_1	load applied to cantilever 1
F_2	load applied to cantilever 2
E_f	corrected flexural modulus
G_I	mode I contribution of strain energy release rate
G_{II}	mode II contribution of strain energy release rate

List of figures

List of tables

1 Introduction

1.1 Background and motivation

Adhesively bonded joints are increasingly being used in aerospace, automotive and maritime industries. The use of adhesive bonding rather than mechanical joining offers the potential for reduced weight and cost. It is important to optimize the joint design and therefore the mechanic properties of the joint must be known. The growth in the industrial usage of adhesive joining brings an economic impact for this optimization that can be very relevant. Furthermore, improving the joint performance has a great influence in the structural toughness of different products for a demanding market with everyday competition.

Fracture mechanics characterization tests for adhesive joints provide relevant mechanical properties to determine the adhesive toughness and guide the design process. Furthermore, the design in terms of durability still needs some research and predict the **energy release rate** after exposure. For example, adhesive joints in automotive applications may be exposed to aggressive environments with high humidity.

1.2 Objectives

The objective of this work is to obtain the strain energy release rate for pure mode I, pure mode II and some mixed-mode I+II combinations in order to obtain a fracture envelope as a function of moisture. The fracture envelope provides information about the fracture toughness that is useful for joint design purposes.

1.3 Research methodology

In order to achieve the aim of this thesis, the following work was done:

1. An overview of some of the most common tests used to characterize the fracture toughness. Some advantages and disadvantages were analyzed for each one. This was followed by a study of the influence of wet conditions in mechanical behavior.
2. A study was done to estimate the water diffusion behavior in the adhesive. Furthermore, a description of materials used and tests performed was made.
3. Numerical simulation was used to predict the water uptake distribution over adhesive the layer. The values used in the numerical simulation was measured using bulk specimen of the adhesive under 50 ºC.
4. DCB and ENF tests were done to characterize the fracture toughness in pure modes of a toughened epoxy adhesive for two different conditions (wet and dry);
5. An apparatus jig was used to predict the fracture toughness over a range of phase angles, since pure mode I to near mode II for two conditions of humidity;
6. The results between the different conditions were gathered to obtain a fracture envelope comparing wet and dry conditions.

1.4 Thesis outline

The structure of the thesis is divided in the following sections:

Chapter 1: A review of adhesive joints and some applications was made, starting by describing the general characteristics of adhesives and the most typical fracture tests to analyze the fracture toughness for each mode. It is followed by a study of principles of water uptake and the influences of moisture in mechanical properties of an adhesive joint.

Chapter 2: Firstly, a description of the specimen and adhesive properties is done. A special description of specimen manufacture was made. A wettability test and a FTIR analysis are described and some phenomena's of water uptake are measured. Testing specifications and particular details are explained for each test mode.

Chapter 3: Moisture concentration distribution is modelled using the software ABAQUS® and the water distribution model for 3 points in the adhesive layer is described. Finite element analysis is described for mode I and mode II to validate experimental results.

Chapter 4: The results are compared and discussed in this section. Diffusion analysis is discussed in order to evaluate the presence of water in the adhesive joint. A comparison of two conditions for each mode is done to verify the accuracy of the experimental results and try to find out a trend in the behavior of the graphs.

2 Literature review

An adhesive joint is a material joining process and consists in the solidification of an adhesive placed between two adherends. This type of mechanical fasteners provide several advantages when compared with other joining technologies such as: lower structural weight; lower cost fabrication; uniform stress distribution over the bonded area which provide the same distribution load and stiffness [1, 2].

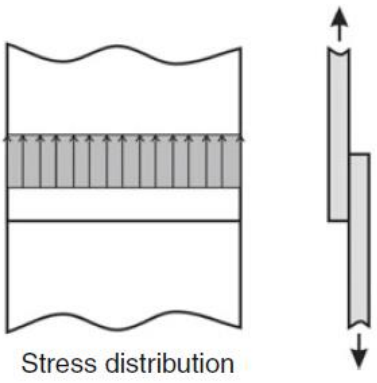

Figure 1: Stress distribution of adhesive joints (adapted from [2]).

However, some disadvantages are associated with adhesive bonding such as the susceptibility to temperature, humidity and solar radiation, presenting limited resistance in extreme conditions. Furthermore, adhesive bonding present some limitation when loaded in tension and the main cases to avoid are cleavage and peel stresses.

2.1 Structural adhesives

An adhesive is named structural if it is able to transfer loads between substrates and generally have a shear strength higher than 5 MPa. Due to a huge variety of adhesives available, the selection an appropriate one requires some experience. A correct fabrication of an adhesive joint is supposed to fail within the adhesive layer.

The selection of an adhesive must consider some factors, such as [2]:

- Joint design;
- Joint performance in terms of load (type, magnitude, operating environment) and durability;
- Substrate type;
- Adhesive form;

- Pretreatments;
- Manufacturing constrains:
- Costs;

The most common adhesives used for structural applications are shown in the next table:

Table 1: Characteristics of different structural adhesives

Adhesive	Characteristics
Epoxy	• High strength • Good toughness • Temperature resistance
Polyurethanes	• Good strength and toughness at low temperatures • Resistant to fatigue • Impact resistance • Good durability
Phenolic	• High hardness • Excellent thermal stability • Limited resistance to thermal shocks • Difficult to process
Silicone	• Environmental stability • High degree of flexibility • Capability to bond materials of various natures • High cost

Thermosetting epoxy resins are largely used as matrix for structural adhesives due to its good mechanical, physical and thermal properties associated with easily processing characteristics [3, 4].

2.2 Adherends properties

Adherend properties have an enormous importance on the joint strength. The design of a joint must take into account the adherend properties and the dimensions. If the adherends have high modulus, the deformation will be lower. In cases of a thin adherend or a low modulus, it is not adequate to select an adhesive of high modulus[5].

Some properties of the most common materials' substrates are presented in Table 2:

Table 2: Common adherends materials properties [6].

Adherend	Young's modulus [GPa]	Tensile strength [MPa]	Elongation at break [%]	Relative density
Hard steel	200	650	25	7.8
Mild steel	205	370	15	7.9
Aluminum	70	275	12	2.7
Carbon fiber (Std. CF)	70	600	0.85	1.6

2.3 Adhesives in transportation industry

2.3.1 Aeronautical industry

Adhesive bonding has found applications in various areas from industries such as aeronautics, aerospace, automotive or naval. This joining technology can lead to a decrease in weight of 15% which drives to improvements in the size and weight of the airplanes. This is directly related to reductions in fuel consumptions and CO_2 emissions per passenger-kilometer [7].

Commercial aircraft benefitted from bonded composite assemblies promoting economical operations because of the reduction of weight, like AIRBUS A380 which lost aproximately 42% of its weight (see Figure 2). However, the difficulties with surface preparation and problems envolving environmental durability make adhesive bonding a non general solution in the aircraft industry [8]. Nowadays, the evolution of the technology increases adhesive applications to more than 345 bonding features in the entire aircraft families.

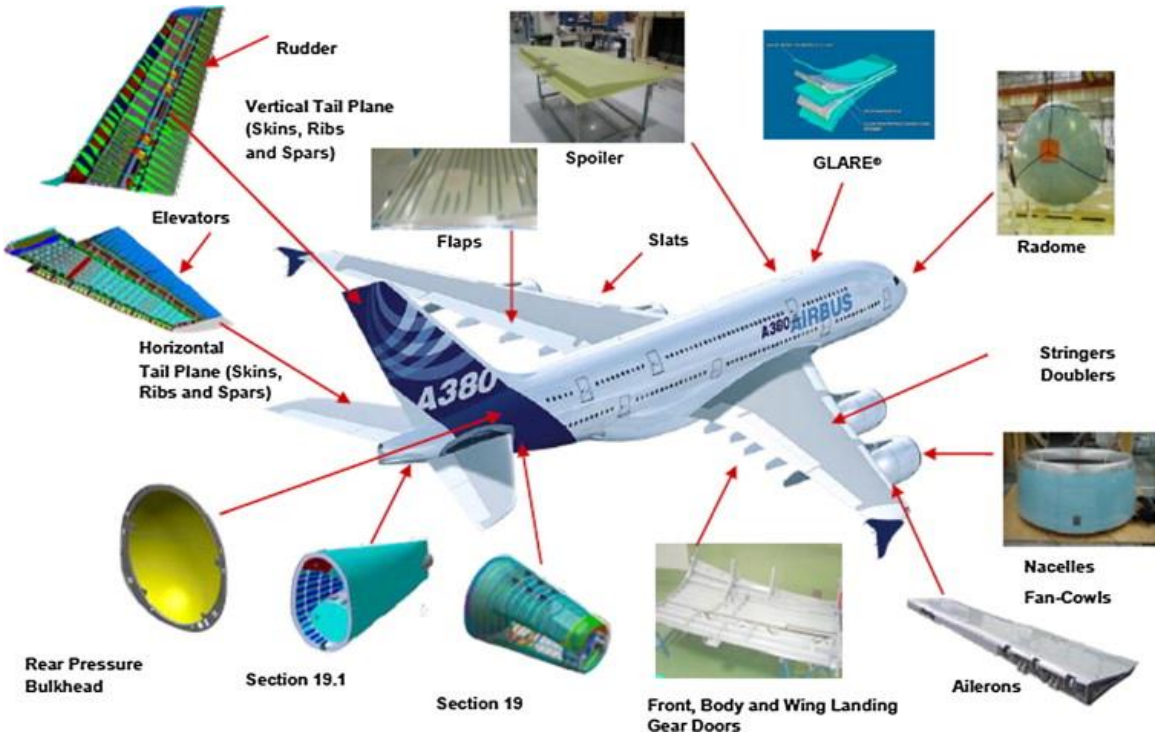

Figure 2: Applications of adhesive bonding at the Airbus A380 [7].

One of the most serious problems about adhesive-bonded construction is moisture-induced failure. This problem was corroborated by experience with the Navy F-4 in South- East Asia which has demonstrated that bonded sandwich panels are susceptible to attack by moisture. As a result, an extensive corrosion of bond line appears, especially in the metal-to-metal area [9].

In addition, some problems related to fatigue of aircraft aluminum structures were shown for some known aircraft incidents such as Aloha Airlines Flight 243 which lost a large part of its fuselage. The Aloha accident got a lot of public attention towards deteriorating safety standards and drew the attention to the importance of the phenomenas of *multiple side damage* (MSD) [10].

Following the recognition of fatigue's phenomena, aircrafts have been designed to prevent the development of cracks during the pre-defined service life, associated with more careful periodic inspections during the service life. Furthermore, some design philosophies were adopted, such as *fail-safe design* and *safe-life design. Fail-safe design* assumes that a component or structure can be safely operated even with some damage, which can propagate until a limit value, and should be withdrawn from service after reaching this value. *Safe-life design* certifies that a component or structure can't develop fatigue cracks during life-service [10].

Following these philosophies, design of metal aerospace components has largely integrated static and yield strength analyses with fracture mechanics, including durability and damage tolerance.

2.3.2 Automotive industry

The use of adhesives in automotive industry starts as a sealer, after that, they were used to prevent corrosion. Nowadays, the applications in car' structures are more common due to the trend to achieve a lightweight design recurring to materials such as Al- and Mg-alloys, sandwich structures or fiber-reinforced plastics [11].

Adhesive bonding is now extensively considered to be a replacement of joining methods such as riveting, bolting and welding for car body joining. The automotive industry aims to maintaining mechanical properties and durability in structural applications [12].

The main advantages in automobile applications are:

- The weight saving;
- Robust and sure structures;
- Uniform distribution of stress and increase of fatigue life;
- Prevention of corrosion between different materials;
- Relatively resistant to impact [11, 12];

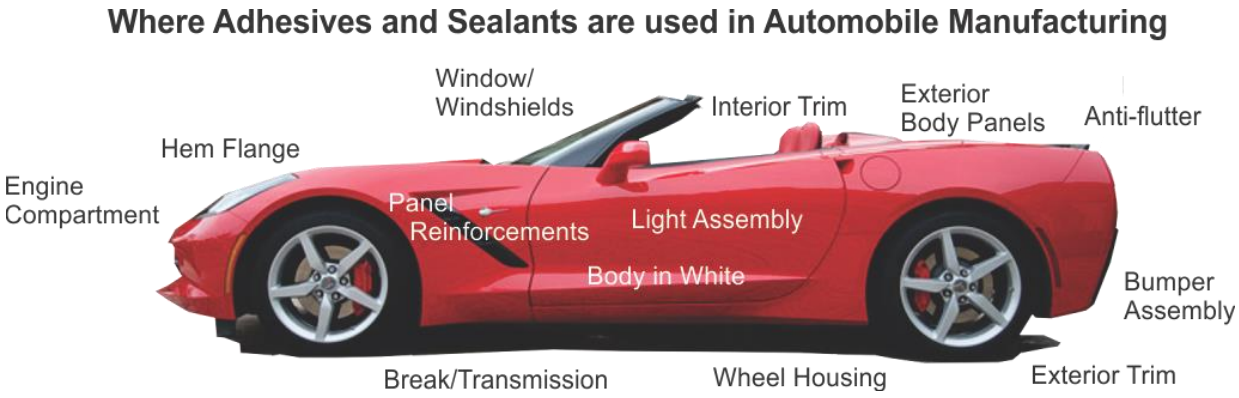

Figure 3: Applications of adhesives and sealants in the automotive manufacturing [13].

2.4 Failure modes

The combination of moisture, heat and mechanical loading are the most damaging effects in the durability of adhesively bonded joints (see Figure 4). For any model of durability of adhesive bonded joints these effects must be considered [14]. According to Davis and McGregor [15] the durability of a bond in service depends of that bond's resistance to degradation in the service environment. For metals like aluminum, hydration is the first cause of degradation. When aluminum is exposed to oxygen, an oxide surface layer appears. After this, if this oxide layer is exposed to water it culminates in hydration. This kind of bond degradation creates an interfacial

failure of the adhesive bond, which means a transition from cohesive failure to a weaker and less predictable mixed-mode failure. The result is a weakening of the bond that is not predictable, quantifiable or easily detectable. However, this phenomena can be prevented with a proper pre-bond preparation of the surface [16].

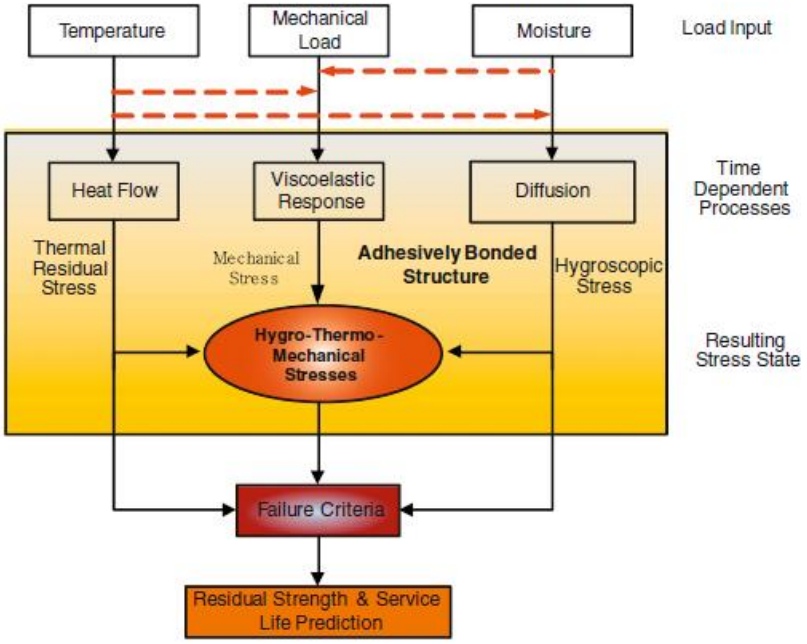

Figure 4: General framework for the durability modelling of adhesively bonded joints [14].

The effect of the environment on adhesively joints is usually investigated, and experimentally the tests are performed using to acceleration of the process with high levels of temperature and humidity. This approach is very useful for comparison of different conditions, however do not provide information for real service conditions.

Nowadays, the best method to predict the effect of the environmental ageing on the properties of an adhesive joint is through hygro-thermal – mechanical finite element analyses. This model is divided in three stages [14]:

1. Determine the moisture distribution in the joint as a function of time from a diffusion analysis;
2. Determine the spatial distribution of mechanical properties;
3. By performing a mechanical analysis, determine the stresses in the joint as a function of ageing time [14].

Failures can occur for several reasons, including uncertainties in the loading or environment, defects in the materials, problems in design or an inadequate maintenance. In order to analyze the failure of an adhesive joint, it is mandatory to identify two types of bond failure:

- *Cohesion failure:* it is achieved if the crack propagates in the adhesive indicating that the adhesive strength is weaker than the substrate's strength and the interface's strength.

- *Adhesion failure*: it happens when bond fails at the interface between adherend an adhesive, and it is typical the interfacial fracture of an adhesive comes with a lower fracture toughness. This type of failure happens for inadequate surface preparation or for ineffective surface preparation process [8];

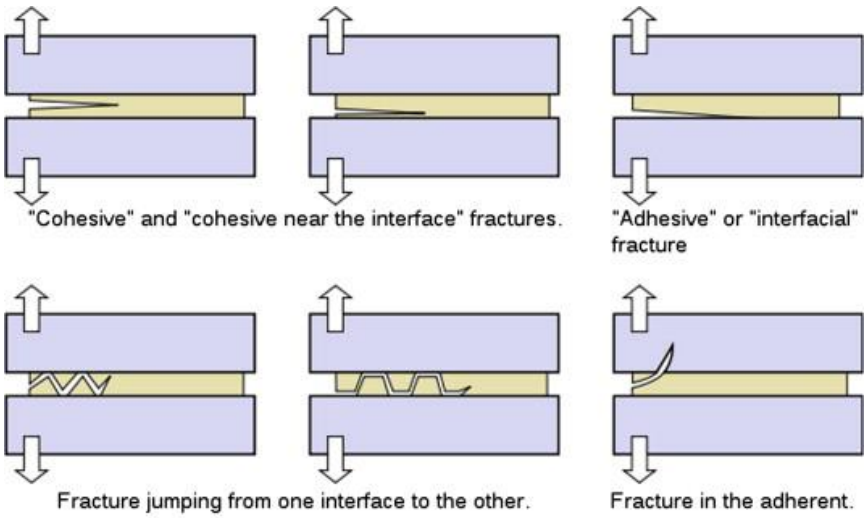

Figure 5: Fracture types [8].

2.5 Strength prediction approaches

The failure of adhesive joints can be characterize by continuum mechanics, fracture mechanics and a combination of both, damage mechanics.

Continuum mechanics approach

A perfect joining between adhesive and adherent is considered based on continuum mechanics. This theory aims to predict the stress and deformations in bonded parts and define the maximal force that can be applied in most common situations :stress, shear, peeling and cleavage (illustrated in Figure 6) [5]. Nevertheless, the singularities inherent to the bonded joint will increase significantly the values obtained for strain and stress [1]. A singularity is a point where stress will achieve an infinite value. This problem can be overcome using a fillet of the adhesive or the adherend, nonetheless the maximum value is dependent on the fillet radius [17].

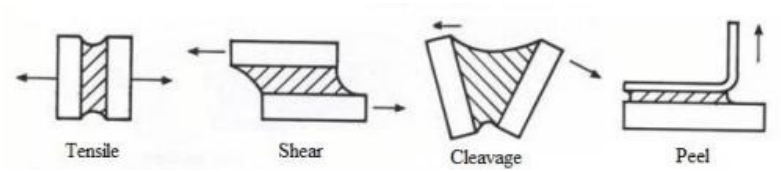

Figure 6: Types of bonded deformations [6].

Fracture mechanics approach

The study of fracture mechanics assumes that the structure behaves like a non-continuous body and has defects or other damages caused during its life at work. Imperfections such as delamination, debonding or cracks are often points of stress concentration and consequently initiation points of fracture which are cause of failure of the component [17]. With this methodology it is intended to evaluate if, during the lifetime of the structure, the dimensions of any defect type remain controlled. This means the dimensions of that defect do not exceed the critical size that would lead to the complete rupture of a structure [18].

There are three different loading modes that can cause a fracture to occur. As shown in figure 7, mode I is an opening mode and mode II and mode III are shearing modes.

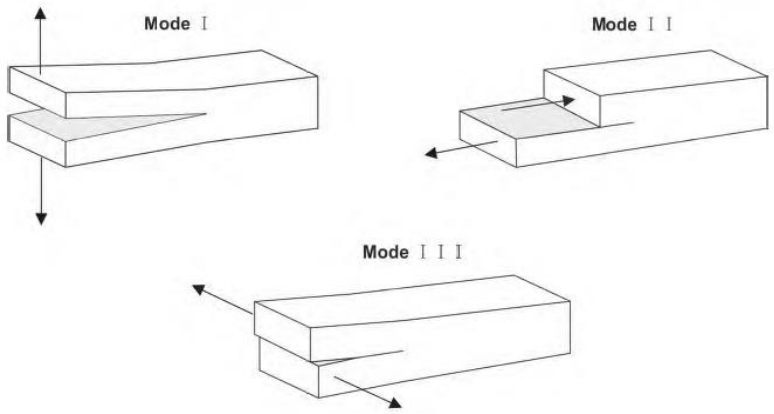

Figure 7: Adhesive joint fracture modes [5].

Stress intensity factor criterion and energetic concepts are used to study fracture mechanics of materials with cracks. The stress intensity factor, *K*, represents a scale parameter that defines the changes in stress state in the neighbourhood of the crack tip [5].

The stress intensity factor, which characterizes the stress at the crack tip, could be represented by:

$$K_I = Y\sigma_r\sqrt{\pi a} \quad \text{Eq. 1}$$

K_I is dependent of Y, a non-dimensional function that depends on the geometry and load distribution and is given for a large number of practical cases; σ_r is a remote stress applied perpendicular to the crack length,α.

When the stress intensity factor is lower or equal to K_{IC}, which is the property that measures the ability to prevent the crack evolution in mode I, it is safe to say that the crack propagation is controlled. The criteria that assures the safety that the crack does not propagate is therefore given by:

$$K_I = K_{Ic} \quad \text{Eq. 2}$$

The propagation of an internal defect will occur when the available energy at that defect's tip, G, is equal to the amount of energy required to promote the crack propagation, G_C, which is a material property:

$$G \leq G_C \quad \text{Eq. 3}$$

On the other hand, the value of K is not easily computed, especially if the crack is located on the interface or in the neighborhood.

Damage mechanics

Damage mechanics is a combination of both continuum and fracture mechanics, and incudes strength and energy parameters to characterize adhesive joint fracture. This is done through an association of properties which represent the mechanical behavior of material with the response to the applied loads. Continuum damage models are appropriate when the thickness has to be considered. One advantage from continuum damage models is to provide information about the thickness' effect in adhesive joints (Figure 12). The fracture process zone changes (FPZ) with thickness and this change causes a different behavior in the adhesive joint fracture [17].

Due to inelastic processes, the FPZ influences the R-curves behavior. These R-curves are graphical representations of the energy release rate variation, G, as a function of the crack length, a. When this curves presents a stabilized plateau as a function of the equivalent crack length, which will be considered the critical energy release rate, the G_c value is obtained [17].

Two cohesive laws are used for the simulations of adhesive joints (Figure 8):

- Trapezoidal cohesive law : This model is used when adhesives have a significant ductility;
- Triangular cohesive law: This is a particular case of trapezoidal cohesive model, adequate for adhesives with brittle and small amount ductile behavior with main advantages of being the easier.

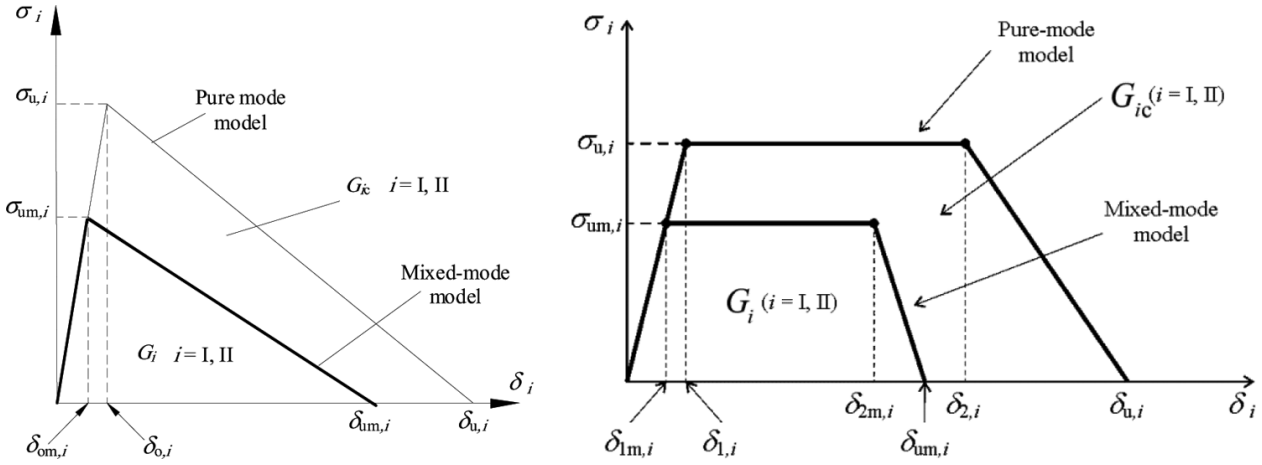

Figure 8: Two typical cohesive laws used in bonded joints [17].

2.6 Fracture mechanics tests

Fracture mechanics tests offer a powerful tool to characterize the failure in adhesive joints. Fracture mechanics has proved being appropriate to demonstrate the structural integrity of bonded systems [11]. Fracture toughness, G_c, is the most relevant property to evaluate for the different mode of loading, which is the energy dissipated during fracture when the crack grows. Fracture varies with the mode of loading, mode I, mode II and for the combination of these modes [5, 17].

2.6.1 Mode I fracture tests

There are two main tests to determine the energy release for mode I:

- Double Cantilever Beam (DCB)
- Tapered Double Cantilever Beam (TDCB)

TDCB is usually used to perform static and fatigue tests, and the achievement of the critical energy release rate is independent of the crack length, however the main disadvantage is the difficult specimen's manufacture compared with DCB.

Double cantilever beam is the most common fracture test, described in the ISO 25217:2009 and ASTM D3433. The specimen (DCB) is comprised of two beams with same length and constant thickness (see Figure 9). The initial part has a region without adhesive, considered to be the pre-crack, a_0, h is the adherent thickness and t is the adhesive thickness. This test measures the fracture strength of an adhesive joint and it is influenced by the adherend's surface conditions, adhesive used in bonding and adhesive-adherend interactions.

Figure 9: Mode I double cantilever beam (DCB) adhesive-joint specimen [2].

The specimen is loaded by opening the beams with speeds between 0.5 and 3 mm/min, which is decided according to geometry and material characteristics. During the test, the load *P* and displacements δ are registered for each crack length, α. The evolution of the strain energy release rate (SERR) *G*, while the test is being executed can be computed using the Irwin- Kies equation:

$$G = \frac{P^2 dC}{2\, da} \qquad \text{Eq. 4}$$

Considering P the applied load, the specimen width b, *C* (C=P/δ) is the compliance and *a* is the crack length.

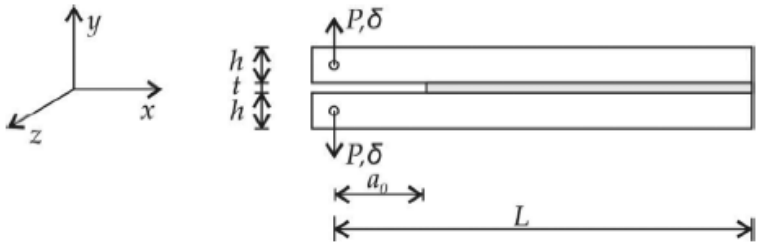

Figure 10: DCB specimen schematics [17].

Compliance-Based Beam Method (CBBM)

The Compliance-Based Beam Method (CBBM) is a data processing technique based on the concept of equivalent crack length, which does not requires the measurement of the crack during the tests. Using the crack equivalent concept, this measurement is irrelevant depending only on the specimen's compliance during the test. The crack length calculated recurring o this method is an equivalent crack length which takes into account the length of the fracture process zone (Figure 12) [17].

Experimentally, the values that need to be registered are load and displacements. The DCB specimen's fracture energy which takes into account root rotation at the crack tip and stress concentration issues is given by:

$$G_{Ic} = \frac{6P^2}{b^2 h^3}\left(\frac{2a_e^2}{E_f} + \frac{h^2}{5G}\right) \qquad \text{Eq. 5}$$

where a_{eq} is the equivalent crack length obtained from the experimental compliance and considering the fracture process zone (FPZ).

The equivalent crack length results from:

$$a_e = a + \Delta a_{FPZ} \quad \text{Eq. 6}$$

The achievement of a crack length needs the solution of the next equation:

$$\alpha a_{eI}^3 + \beta a_{eI} + \gamma = 0 \quad \text{Eq. 7}$$

The values of α and β are given by:

$$\alpha = \frac{8}{Bh^3E}; \quad \beta = \frac{12}{5BhG}; \quad \gamma = -C_1 \quad \text{Eq. 8}$$

$$A = \left(\left(1 - 108\gamma + 12\sqrt{3\frac{(4\beta^3 + 27\gamma^2\alpha)}{\alpha}} \right)\alpha^2 \right)^{1/3}$$

The equivalent flexural module, E_f is obtained from:

$$E_f = \left(C_0 - \frac{12(a_0 + |\Delta|}{5BhG_{LR}} \right)^{-1} \frac{8(a_0 + |\Delta|)^3}{Bh^3} \quad \text{Eq. 9}$$

Where Δ is the root rotation effect at the crack tip and can be given by:

$$\Delta = h\sqrt{\frac{E_f}{11G_{LR}}\left[3 - 2\left(\frac{\Gamma}{1+\Gamma}\right)^2\right]} \quad \text{Eq. 10}$$

And:

$$\Gamma = 1.18\frac{E}{G} \quad \text{Eq. 11}$$

2.6.2 Mode II fracture tests

There are several tests allowing the determination of the mode II fracture toughness of adhesive joints such as:

- ENF (End Notched Flexure)
- ELS (End Loaded Split)
- 4ENF (Four-point End Notched Flexure)

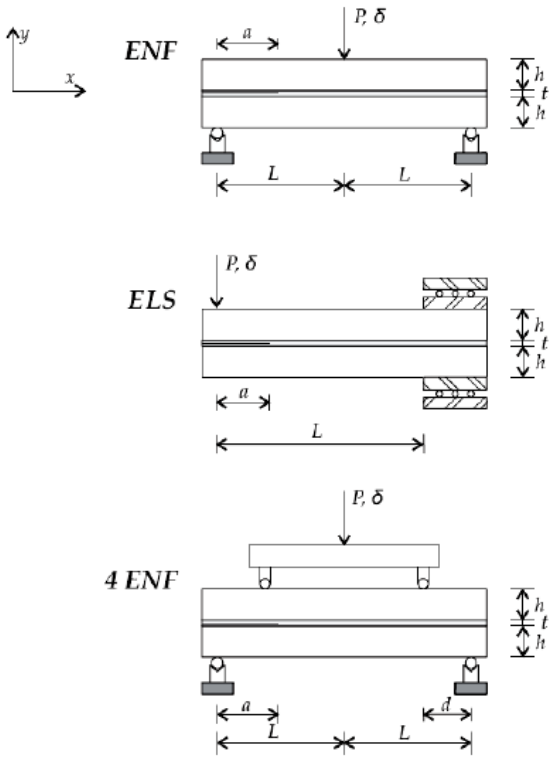

Figure 11: Best known mode II tests for characterization of adhesive joints [5].

ELS presents some difficulties to the determination of a correct value to G_{IIc} related to the existence of large displacements and some sensitivity to the clamping. However, this fracture tests bring some advantages because promotes a stable crack initiation. The 4ENF test is the most sophisticated test, despite presenting some friction problems at the pre-crack zone as result of loading.

ENF test is the most common to obtain the mode II fracture toughness of an adhesive joint as result of being the simplest.

This fracture test consists of two beams with constant thickness bonded along its length, with exception of the pre-crack region, and with two simple supports at the extremities. A load is applied in the middle of the length instigating shear in the adhesive. Using the beam theory and Irwin-Keyes equation, and not taking into account the transverse shear effect at the crack tip, G_{II} can be get by:

$$G_{II} = \frac{9P^2a^2}{16b^2Eh^3} \qquad \text{Eq. 12}$$

To fix this another equation take into account the root rotation at the crack tip:

$$G_{IIc} = \frac{9P^2(a + |\Delta_{II}|)^2}{16b^2Eh^3}$$ Eq. 13

Where Δ_{II} correspond to crack length correction, and is related to crack length for mode I with DCB test, Δ_I :

$$\Delta_{II} = 0.42\Delta_I$$ Eq. 14

The main disadvantages of these methods are the necessity of monitoring the crack growth during the test, which presents difficulties because the crack propagation occurs by shear with adherends in contact. Furthermore, the fact of not taking into account the Fracture Process Zone (FPZ) at the crack tip is another drawback.

As mentioned before, ENF has some problems related to crack measurement during the propagation, because it is difficult to visualize it. In addition, some aspects related to FPZ cause different behaviors when fracture of adhesive joints occur as a function of different thicknesses. FPZ is defined as a region near the crack tip, as shown in Figure 12, where inelastic processes happen, like micro-cracking and plastic micro straining. This energy has to be considered, so another value appears: equivalent crack length which takes into account he inelastic processes mentioned before. The FPZ is considered in the definition of compliance [19]:

$$C = \frac{3(a + \Delta a_{FPZ})^3 + 2L^3}{12E_f I} + \frac{3L}{10Gbh}$$ Eq. 15

To get the equivalent flexural modulus:

$$E_f = \frac{3a_0^3 + 2L^3}{12I}(C_0 - \frac{3L}{10Gbh})^{-1}$$ Eq. 16

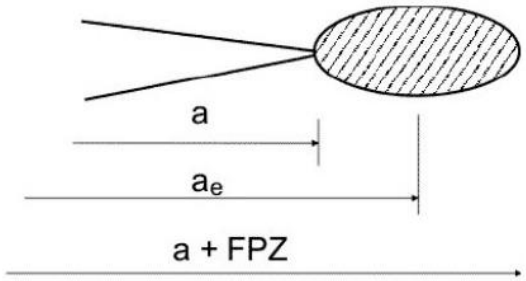

Figure 12: Definition of FPZ and equivalent crack length [5].

2.6.3 Mixed-mode

The mixed-mode criteria appears in the way that the most common situations, the loads applied are a combination, at same time, of peeling and shear stresses.

There are several tests to characterize the behavior of the adhesive joints in mixed mode:

- Single Leg Bending (SLB)
- Asymmetric Tapered Double Cantilever Beam (ATDCB)
- Asymmetric Double Cantilever Beam (ADCB)
- Cracked Lap Shear (CLS)
- Mixed Mode Bending (MMB)

MMB test is the only standard test available to evaluate the mixed-mode toughness of a composite (defined in ASTM D6671). This test consist in the combination of the two most important tests to get the characterization of the toughness in mode I and mode II, DCB and ENF respectively. As shown in Figure 13, an opening load is add to the ENF test:

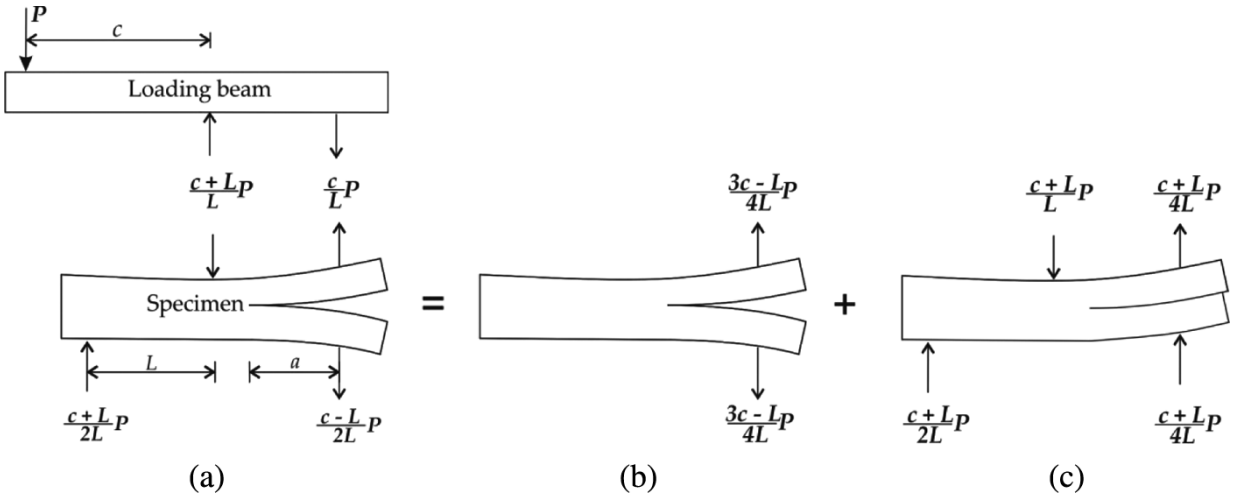

Figure 13: MMB free body diagram [5].

The MMB is included in ASTM standards, however it was developed for delamination in composites specimens and it is of difficult application for aluminum or steel specimens [6].

Table 3 shows different tests schemes with a dissimilar ratio of ratio.

Table 3: Mode ratio for different mode ratio tests [17].

Test	Tset scheme	Global mixity, ψ (degree)
Asymmetric double cantilever beam (ADCB)	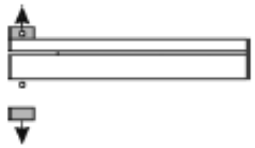	≈ 0–34°
Single leg bending (SLB)	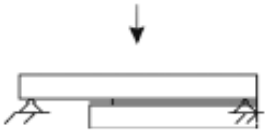	≈ 41°
Crack lap shear (CLS)		≈ 49°
Asymmetric tapered double cantilever beam (ATDCB)	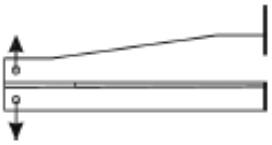	≈ 20°
Mixed-mode bending (MMB)	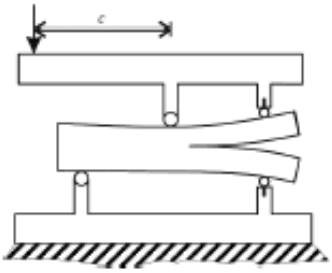	$\psi = f(c)$
Spelt loading jig (SPELT)	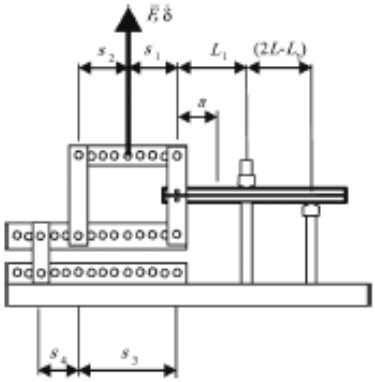	$\psi = f(s_1, s_2, s_3, s_4)$

The characterization of mixed-mode fracture ratio in planar problems is governed by:

$$\varphi = tan^{-1}\left[\frac{K_{II}}{K_I}\right] = tan^{-1}\sqrt{\left(\frac{G_{II}}{G_I}\right)} \qquad \text{Eq. 17}$$

Fracture envelope

The first reason for conducting mixed mode fracture tests is to generate a more complete understanding of an adhesive bond's behavior resistance to fracture over a range of loading combinations [20].

Chaves et al.[21] characterized the fracture of bonded joints under different mixed-mode I+II loading conditions based on specimen compliance, beam theory and crack equivalent concept. Figure 14 presents seven scenarios analyzed having in consideration two criterions: linear and quadratic criteria.

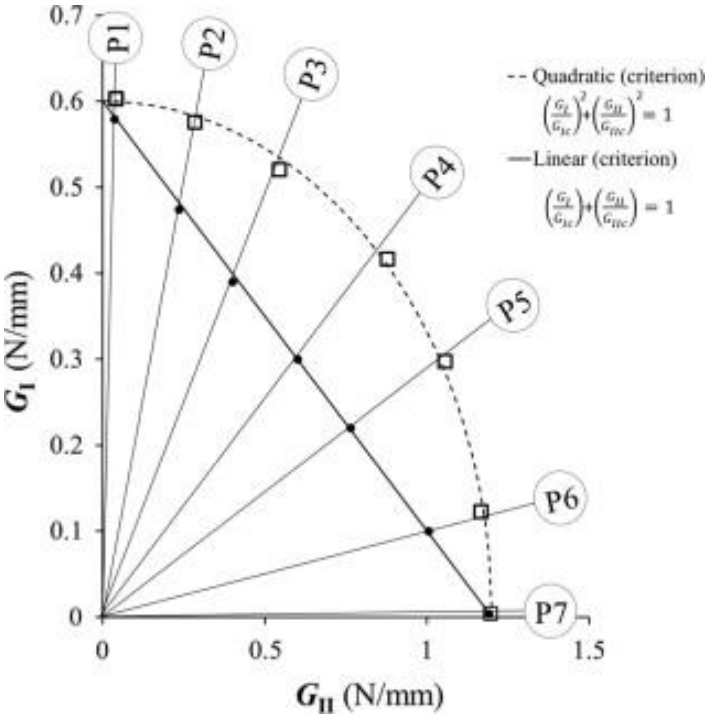

Scenarios	Jig arrangement			
	s_1 (mm)	s_2 (mm)	s_3 (mm)	s_4 (mm)
P1	100	40	140	−60
P2	120	40	160	−120
P3	40	120	160	40
P4	60	80	140	60
P5	60	80	140	120
P6	40	40	80	100
P7	100	40	140	80

Figure 14:Fracture envelope for the seven scenarios [21].

An apparatus (Figure 15) was developed for measuring the toughness of adhesive joints in a wide range of fracture modes from mode I (opening mode) to mode II (shear mode) depending on the load-displacement curve. The *P-δ* curve is obtained from an universal testing machine and two LVDTs (linear variable differential transformer) connected to each beam [5].

Figure 15: Mixed-Mode apparatus.

This loading jig presents some advantages from another solutions, such as:

- this invention places the specimen inside its structure which reduces the dimensions and the space need for testing;
- it is not necessary to measure the crack, because it uses the displacement obtained from the LVDTs.

2.7 Effect of environmental moisture on adhesively bonded joints

2.7.1 Principles of water uptake

Currently, adhesive bonding is used in many applications in automobiles, however one of the main concerns when using adhesive joints in a structure is that the adhesive can absorb water from the surrounding environment. The water uptake affects mechanical properties of bulk adhesive and also the integrity of the adherend.

Diffusion of moisture is a time dependent process, which is driven by a concentration gradient, transport water from one place to another. This process is a function of water concentration, time, sheet thickness and temperature [22].

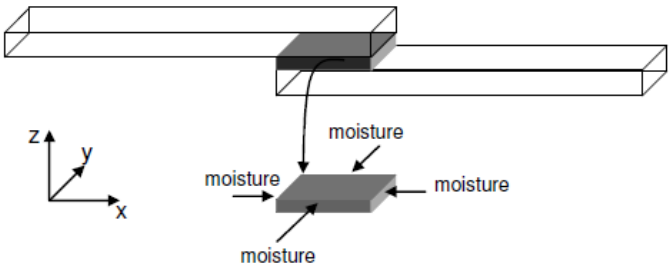

Figure 16: Moisture diffusion in the adhesive layer of a single lap joint [22].

The diffusion of water happens from "both sides perpendicular to the thickness" (Figure 16) and the flux of moisture into the polymer can be described by Fick's first law [22, 23]:

$$F_x = -D\frac{dc}{dx} \qquad \text{Eq. 18}$$

where F_x is the flux of moisture, D is the coefficient of moisture diffusion and x is the diffusion direction [22, 23].

The concentration of moisture as function of time can be defined by Fick's second law:

$$\frac{\partial c}{\partial t} = D\frac{\partial^2 c}{\partial x^2} \qquad \text{Eq. 19}$$

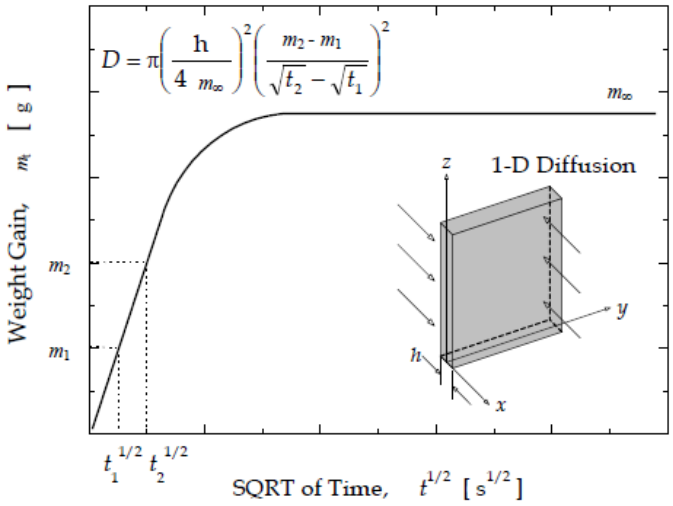

Figure 17: Theoretical curve of weight for one dimension Fickian behavior [23].

Figure 17 shows the theoretical absorption curve for a Fickian diffusion. Diffusion plots are obtained from weight gain as a function of square root of time. The diffusion coefficient is obtained from the slope of this curve [23]:

$$D = \left(\frac{M_t}{M_\infty}\right)^2 \times \frac{\pi}{16} \times \frac{h^2}{t} \qquad \text{Eq. 20}$$

where M_t is the relative mass uptake and M_∞ is the saturation level (in %) [23].

In an adhesive joint, the water's absorption could take different ways, such as diffusion in the bulk adhesive, transport along the interface, diffusion through the adherend in cases of permeability to the water and the existence of cracks and crazes facilitate the flow of water [22].

Based on the assumption that the temperature at which an adhesive joint will be tested is not always room temperature, it is necessary to study water uptake for higher temperatures. Shen and Springer propose that the temperature doesn't influence significantly the maximum water content and this value depends on moisture content environment. However, to reach the

maximum value of water content with a higher speed, the temperature must be raised and the water in the surrounding doesn't influence the results [24].

Loh et al. [25] suggested that epoxide adhesives can absorb water up to a maximum of about 10% moisture by mass, and this value can change for different exposure time, stress state, water concentration, temperature, chemical nature and structure [25].

The diffusion of water into epoxy-based adhesives can lead to a swelling phenomenon. This is a specific material's response associated to water diffusion. This phenomenon is verified when "the volume of the resin-containing water is less than that of the volume of the water absorbed plus the volume of dry resin"[26]. Swelling can change with concentration and temperature [26].

The effects of water uptake could be plasticization of the adhesive and adherend (in some cases), the weakening of the interface and swelling. This will affect mechanical properties, the internal stresses distribution and potentially the failure criterion [2]. Some effects, such swelling and plasticization are reversible. Nonetheless, micro-cracking and hydrolysis stimulates the degradation of adhesive properties (mechanical, thermal and physic-chemical) [4].

2.7.2 Influences of water uptake in the adhesive properties

According to Liljedahl et al. [27] the main disadvantage of using adhesives is related with humid environments. The environment exposure leads to a significant decrease of mechanical and thermomechanical properties in bonded joints [23]. A consistent knowledge of the mechanisms of the moisture ingress would lead to greater confidence and thus increase the use of the adhesives [27]. The bonding durability is extremely dependent upon the adherends, surface preparation adhesive/primer system and environment [16].

The mechanisms that cause degradation can occur before, during and after preparation or cure of a joint. One of the possible causes of degradation of joint strength is related with the contact with atmospheric moisture. The joint fails cohesively under dry conditions, while the interface fails in wet environments. However, some adhesives are more susceptible than others to the surrounding environments and the amount of degradation also diverges [28].

Most of adhesives are hydrophilic, what means that they absorb moisture. The absorption of water can reduce the glass transition temperature (T_g) and decrease the mechanical strength

[28]. Barbosa et al. [4] observed the effect of hygrothermal aging in the mechanical properties of an epoxy system and it was also verified a decrease of Young's modulus and tensile stress.

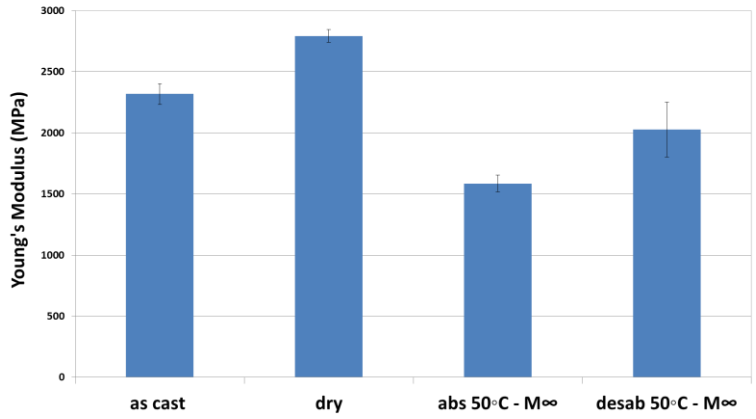

Figure 18: Young's modulus of specimens with different moisture stages (adapted from [4]).

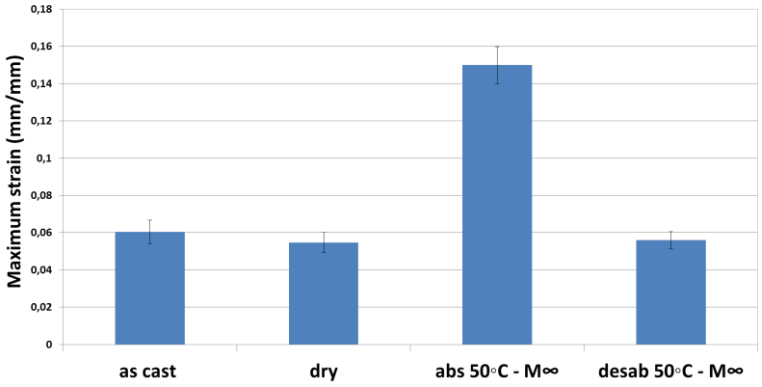

Figure 19: Maximum strain of specimens with different moisture stages(adapted from [4]).

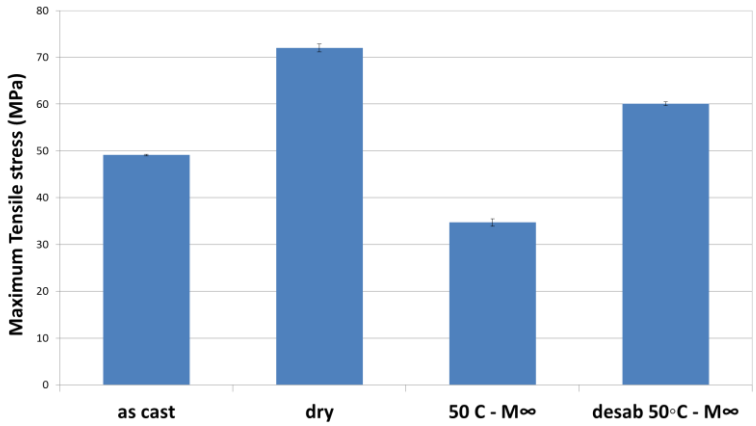

Figure 20: Maximum tensile stress with different moisture stages (adapted from [4]).

As shown in Figure 18 and Figure 19, the mechanical properties, such as Young's modulus and the maximum stress decreases when the water temperature increases. Moreover, it is verified an increasing in the plasticization, however this phenomenon is reversible by drying.

Figure 21 presents the stress- strain curves of an epoxy adhesive (after cured), used for automotive applications, during 2000 hours for room temperature, 40ºC and 60ºC. The decreasing in Young's modulus and maximum stress as the water temperature increases is verified. Hot water increases significantly the plasticization. However, this effect of water uptake is reversible [29].

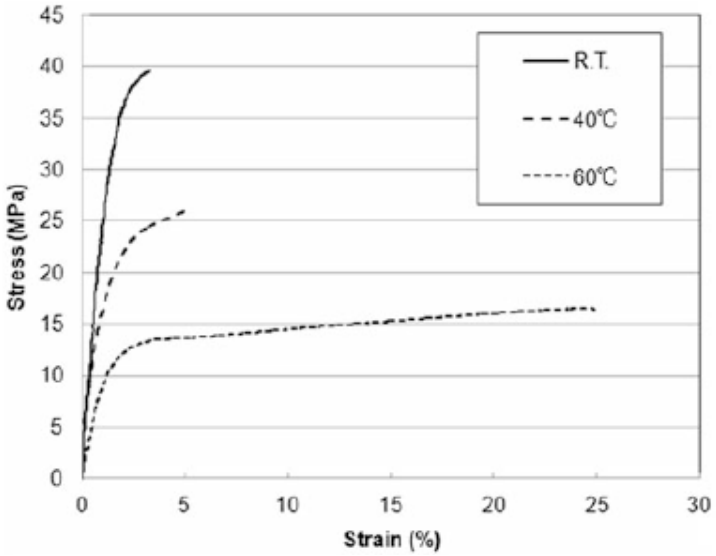

Figure 21: Stress strain curves of an epoxy system at different temperatures in water [14].

Thermosetting epoxy resins have two behaviors for moisture absorption. This stages are more visible when decreasing the thickness. From Figure 22 shows that for different thicknesses the first stage followed the Fick's law and the slopes are very similar for all the curves. Furthermore, a second behavior is detected and the diffusion coefficient is meaningfully lower than the first behavior.

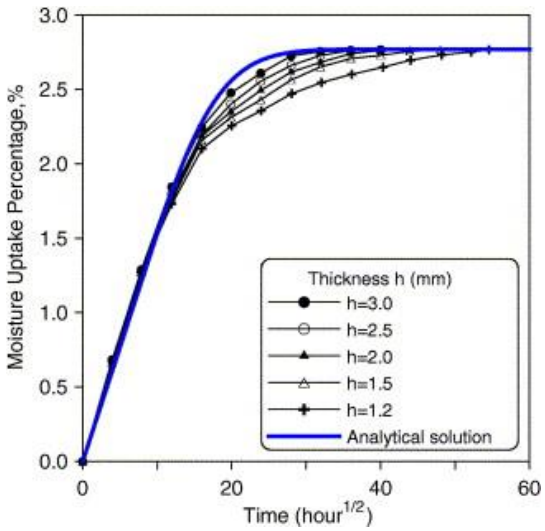

Figure 22: Moisture Uptake Percentage as function of different thicknesses [3].

2.7.2.1 Fracture toughness

The water uptake into the adhesive causes a reduction in the stress-strain response [22]. Katsiropoulos e al. studied the mechanical performance of two epoxy adhesives. A comparison between them has been performed: the effect of thermal aging and the adhesive thickness on the fracture toughness of an adhesive joint [8].

As show in Figure 23, LMB Huntsman adhesive, an advanced prototype two-part paste epoxy, and Epibond 1590 A/B adhesive, an aerospace two-part paste were tested in mode I and mode II. The effect of wet-ageing for mode I is the increase of the G_{Ic} for both adhesives with a thickness of 0.5mm. Furthermore, a decreasing of mode II is verified in consequence of the water uptake for LMB adhesive for thickness 1 [8].

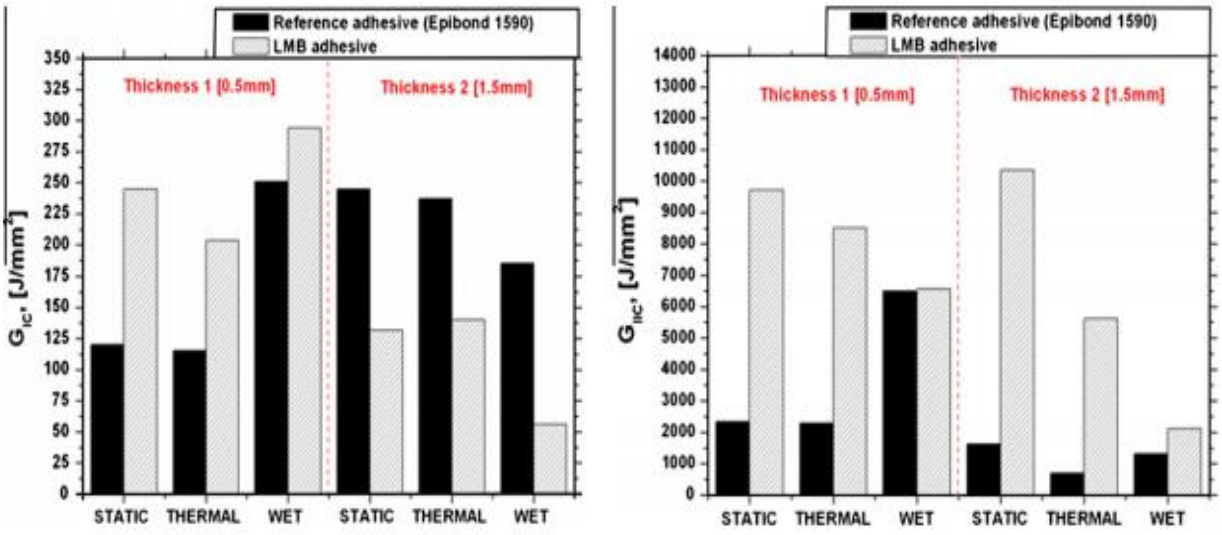

Figure 23: Comparison between mode I and mode II after ageing for epoxies adhesive [1].

Loh et al (2002) suggested that that the fracture load decreased with an increase of moisture content (see Figure 24). The mixed mode toughness with adhesive AV119 was studied and "when the load reaches a critical value, the crack starts to propagate and the load drops due to an increase in the specimen compliance". The fracture energy presented a highly decrease for higher levels of water uptake [22, 30].

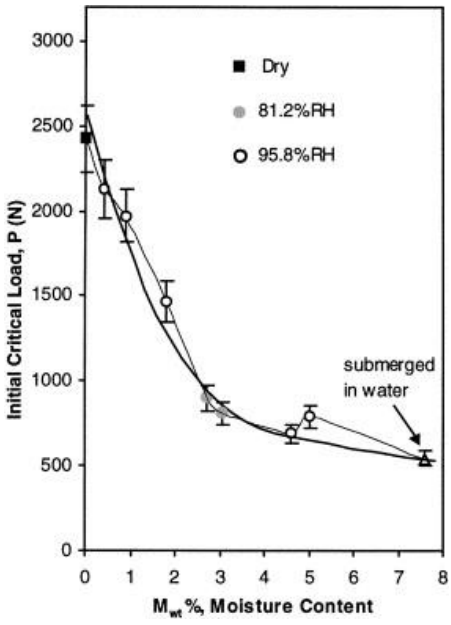

Figure 24: Initial peak load as function of moisture [30].

Wylde and Spelt tested the fracture of two toughened epoxy adhesives, Cybond 1126 and Cybond 1126 in wet and dried conditions. They have observed that the existence of water in the adhesive for wet conditions, increases the joint fracture toughness [31].

The same authors also studied G_c for a mixed mode combination (φ) of 60° and 48° as function of the exposure time at 100% relative humidity and 35 °C for both wet and dry conditions. For wet conditions, they verified an increase of G_c after 30 days of ageing. After these 30 days a decreasing was measured. The mixed mode combinations shown the same behavior for wet conditions. It was noted that for longer exposure times, the effects of plasticization became not so important as degradation progressed.

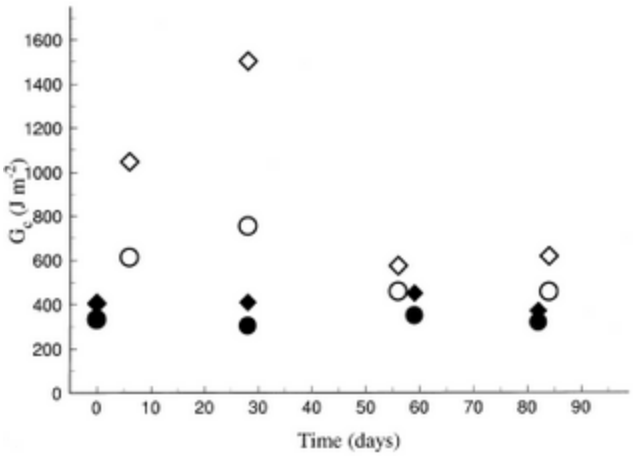

Figure 25: G_c versus exposure time for Cybond 4523GB degraded 100% relative humidity φ=48º (○) and φ=60º (□) (wet) and in dry conditions φ=48º (•) and φ=60º (♦) [31].

Figure 26 represents the evolution of fracture toughness as function of time spent ageing for a temperature of 65 ºC. The mixed mode fracture toughness presents an increasing with time spent ageing [31].

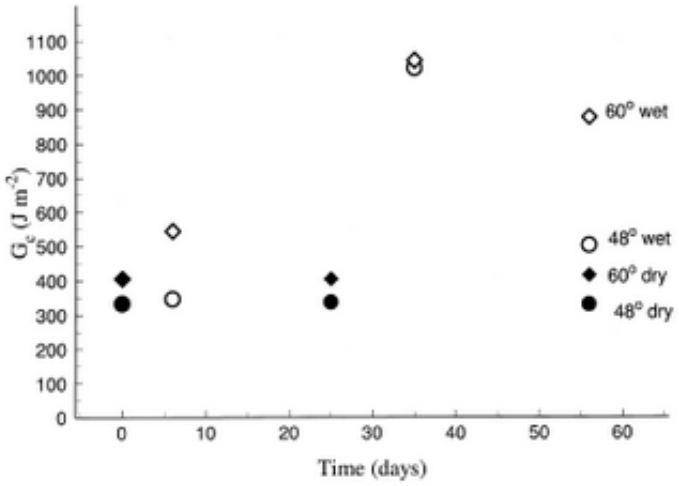

Figure 26: G_c versus exposure time for an epoxy system degraded at 100% for two mixed mode combinations at 65 ºC [31] .

Sugiman [22] showed that epoxy adhesives such as AF-191U and FM73U which have been aged in wet environments show a decrease in modulus, tensile strength, and also fracture toughness, although the maximum strain increases.

Lapland at al. [32] tested an high-temperature epoxy adhesive for mode I, FM300 structural film adhesive. The results of this investigation present a higher value for fracture toughness with increase of the moisture content. According to the author this values were expected in consequence of plasticization after water uptake. However the increasing of fracture toughness presented higher values for 1% of moisture content than with 3%. This is justified by a lower molecular mobility reflected in lower relaxation rate.

Ameli et al. [33] verified the variation of degraded mixed mode toughness for two phase angles of 27º and 48º in function of degraded mode I. As shown in Figure 27 the values for degraded mixed mode are proportional with mode I. For a high value of ratio's combination, the slope has a high value.

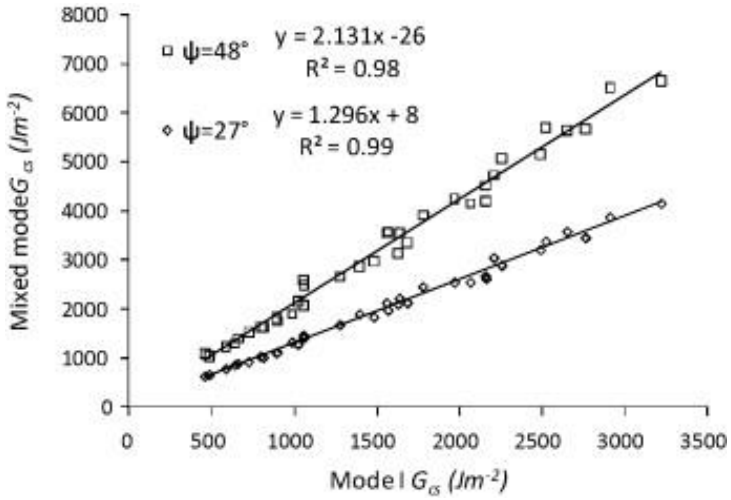

Figure 27: Degraded mixed-mode values G_{cs} as function of mode I [34] .

Cheng Li et al. [35] concluded that "the failure mechanisms are complex and involve a combination of plasticization, stress relaxation of the adhesive and destabilization of the interface by conversion of the oxide into hydroxide".

2.7.3 Surface treatment

Before adhesive bonding some concerns have to be considered, namely the moisture that will be absorbed decreasing the adhesion. This absorption decreases the strength between adhesive and adherend which leads to another cause of failure. However, a good surface preparation can reduce the interfacial debonding.

The use of metallic adherends in an adhesive joint, requires a surface treatment to provide a high performance and a durable adhesion during the service life of the structure. There are different surface treatments for a different adherend. The efficiency of surface treatment is dependent of a large number of factors such as mechanical loading and the environment, besides the selection must fit the needs of the project [14].

The extensive use of aluminum alloys in the transportation industry and the problems in joining them results in many studies to optimize their surface treatments. In order to have a good preparation, aluminum alloys need to be carefully treated with the main purpose of improving "the quality of bonded metal joints by removing the contaminants, controlling the oxide formation, bridging the adherend and adhesive, and controlling the surface roughness" [22].

There are many surface treatment methods, nevertheless, as illustrated in the figure 26 phosphoric acid-anodized (PAA) provides a lower crack growth and more durability than chromic acid etch (CAE) and chromic acid-anodized (CAA). This happens due to the formation of a very porous oxide coating which leads to a highly adherent surface [22]. Chromic acid anodising also produces a porous oxide and a corrosion protection, however is a dangerous anodising process[14].

This conclusions comes from "Boeing" wedge-test, which is a quick control technique for evaluating the adequacy of the adherend surface treatment for epoxy/aluminum alloy joints with three surface treatments (Figure 25).This test measure a crack growth, $\Delta\alpha$, which can not exceed the initial crack length after exposing to a wet environment [36]

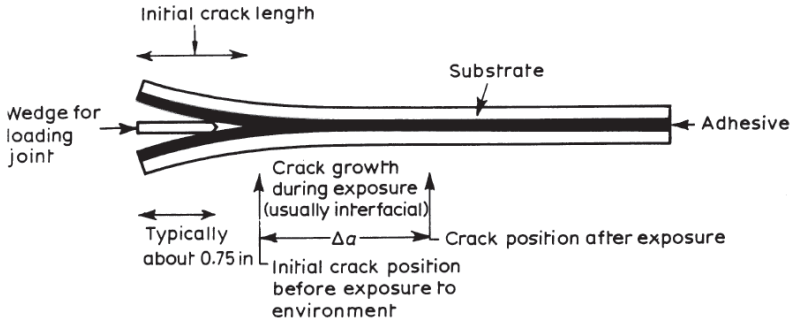

Figure 28: The Boeing wedge-test for assessing joint durability [36].

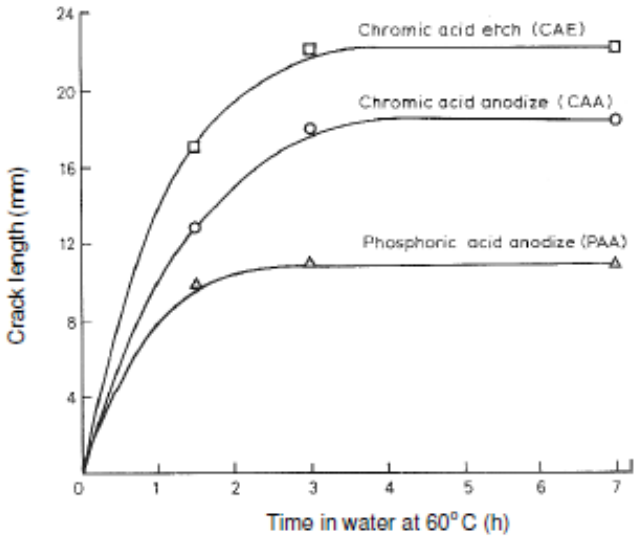

Figure 29: Effect of surface treatments on the crack growth of aluminum joints [36].

The anodization process is a coating process "where the metal forms the anode in an electrolytic cell and the applied voltage effectively drives the process to increase the thickness of the converted layer on the surface of metal parts". Figure 30 shows the ideal anodic coating on aluminum [14].

The anodic oxide film is dependent of many factors such as:

- The alloy used;
- Any pre-process such etching;
- The electrolyte used;
- Anodising temperature;
- Voltage conditions;
- Anodising time;
- Post-treatments (like etching or sealing)[14].

A moisture-rich environment causes a bigger reduction in fracture energy when compared with a dry environment and increasing temperature will lead to a faster degradation, as result of the moisture diffusion [16].

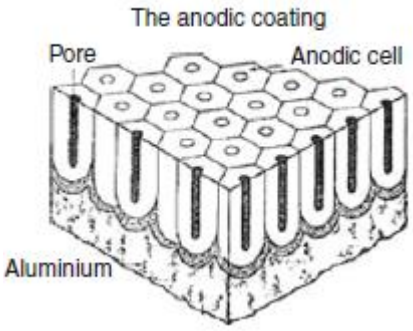

Figure 30: Pores after PAA on aluminum [2].

Damage mechanics approaches discussed above to predict the environmental degradation in adhesive bonded joints must be integrated into a durability modeling framework. In order to define environmental degradation modelling of bonded joints, finite element analysis combined with one of the progressive damage models must be considered. This approach includes three important steps. The first step is modelling transport through the joint aiming to find the moisture concentration distribution in the joint as a function of time. The next step includes the determination of the transient mechanical-hydro-thermal stress-strain state according to results from combined effects of hydro-thermal and mechanical loads. The last step is the mixture of damage processes with the purpose of modelling the progressive failure of the joint and predict the residual strength or lifetime [14].

3 Experimental details

3.1 Adherend

The adherends material used to manufacture DCB adherends is aluminum Al7075-T6 supplied by Lanema (Ovar, Portugal). The choice of this aluminum is related with the yield strength, σ_y, which assures that is high enough to avoid any plastic deformation during the tests. The general properties of the aluminum used are presented in Table 4.

Table 4: Mechanical properties of aluminum 7075.

Maximum strength (Rm)	Yield strength (Rp 0,2)	Hardness (Brinell)
525 MPa	455 MPa	130-150

3.1.1 Specimens geometry

The DCB geometry used is represented in Figure 31.

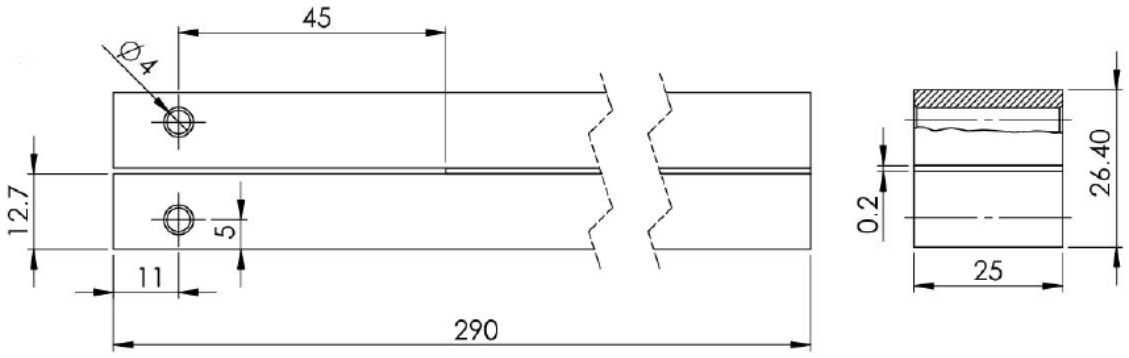

Figure 31: DCB geometry [37].

3.2 Adhesive

3.2.1 *Nagase XNR 685E-2*

Nagase XNR 685E-2 is a prototype developed by NAGASE CHEMTEX® (Osaka, Japan). This adhesive is composed of one component and it's an epoxy adhesive. Epoxy resins are commonly used for structural applications due to good mechanical properties [20]. This structural adhesive fits the requirements of automotive structure applications.

This adhesive cures at 150˚C during 3h50. The stress-strain curve is shown in Figure 32.This test was performed at room temperature and with a constant displacement rate of 1 mm/min.

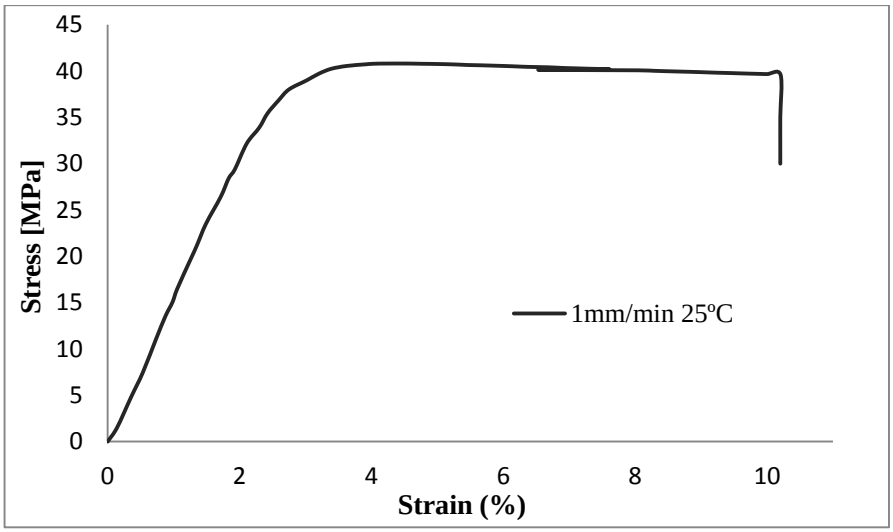

Figure 32: Stress-strain curve of Nagase XNR 685E-2.

Table 5: Mechanical properties of the adhesive at room temperature.

Young's modulus (MPa)	Tensile strength (MPa)	Strain failure (%)
1742 ± 134	42.9 ± 1.9	9.95±4.01

The adhesive used for the manufacturing of DCB's and bulk specimens Nagase XNR 6852E-2 has to be pre- heated in an oven at a temperature of 50 ˚C during 20 minutes. After this, the adhesive was placed inside a recipient in a centrifuge mixing machine, a SpeedMixer DAC 150^{TM} (Hauchild, Hamm, Germany), for 1 minute at 3500 rpm to get a homogenous mixture.

3.3 Specimen manufacture

The specimen manufacture is an important phase to promote cohesive failure and obtain good results from the tests. The specimen geometry is in accordance with the ASTM 3433-99. The geometry of the DCB test specimen is given in Figure 33. The main goal of this step is to ensure that adhesive rupture, this means avoid the break at the interface. The tests require double cantilever beam specimens and some steps have to be done:

1. Mold preparation;
2. Substrate preparation;
3. Adhesive deposition;
4. Hydraulic press;
5. Curing of the adhesive;
6. Removal and cleaning;
7. Preparation for testing

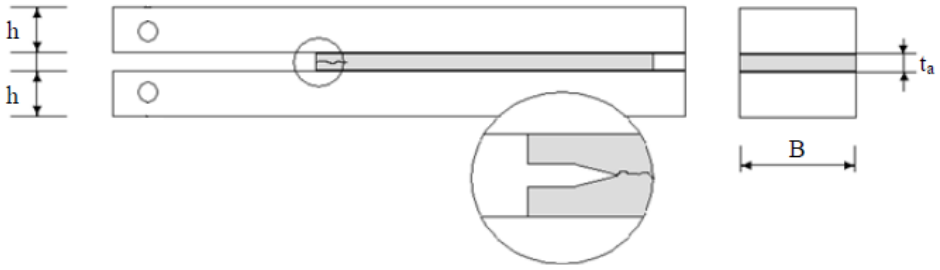

Figure 33: Schematic of DCB specimens [38].

3.3.1 Mold preparation

The mold surface must be cleaned, removing any trace of adhesive using acetone and paper sheet. After cleaning, a release agent (FREKOTE 770NC) was used to prevent adhesive bonding with the mold.

3.3.2 Substrate preparation

The surfaces preparation is an important step in the adhesive bonding to assure the quality of the joint.

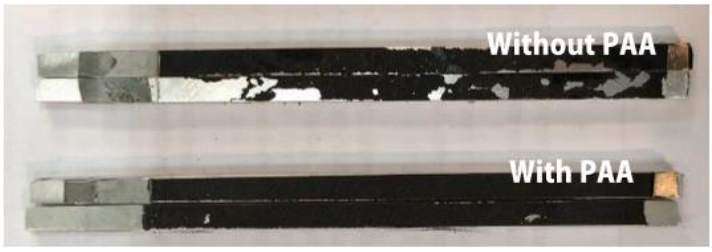

Figure 34: Difference between use or not PAA in aluminum specimens [2].

The preparation of the aluminum surfaces for structural adhesive bonding followed the ASTM D3933. This surface preparation provides a stable oxide coating, with many pores, as shown in Figure 30, allowing the primer to penetrate.

The main steps for the phosphoric acid-anodizing are:

- Surfaces of the adherends were grit blasted;
- Surfaces were degreased with acetone, removing the impurities resulting from grit blasting;
- Solution was prepared with 12% concentration of phosphoric acid and distilled water (agitate the solution);
- The aluminum specimens were dipped in the solution and the electric circuit was prepared according to Figure 35;
- The prepared electric system is adequate to produce 16 V and the terminals were positioned so that the parts are not in contact with the solution;

- The anodization process should be performed continuously during 20 to 25 min;
- The specimens were cleaned using a source of water;
- The specimens were dried in air and each one involved in an aluminum sheet;
- The manufacturing of DCB's has to be done up to 72 hours after the surface treatment.

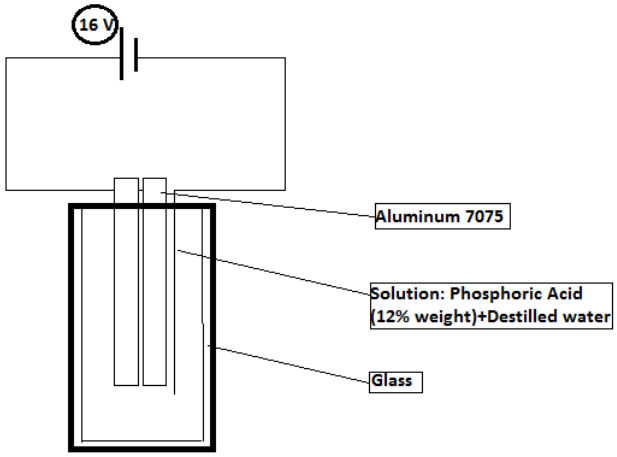

Figure 35: Schematic illustration of PAA.

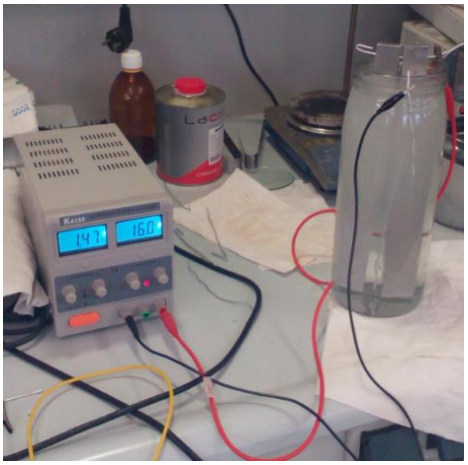

Figure 36: Execution of the PAA.

3.3.3 Adhesive deposition

To guarantee the adhesive thickness, spacers were inserted between the adherends on both ends (Figure 37). Adhesive was applied in both adherends before assembly and then set in a mold for correct alignment.

In the first extremity two steel plates of 0.05 mm and a razor blade of 0.1mm were inserted to introduce a pre- crack and guarantee a cohesive propagation of the crack during the test. On the other end a feeler gauge was used to assure a thickness of 0.2 mm. If the adhesive thickness is too low for full development of a plastic zone, the fracture toughness will be different. Furthermore, the automotive industry use 0.2 mm thickness.

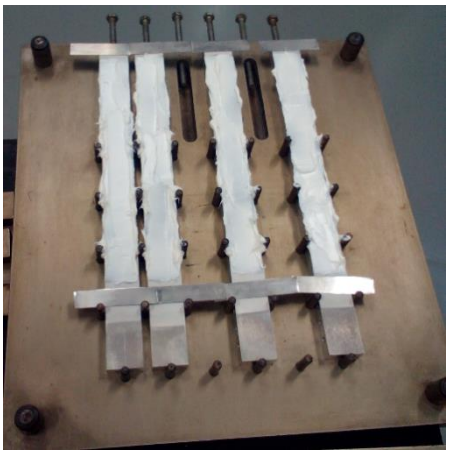

Figure 37: Adhesive deposition and spacer's alignment.

3.3.4 Hydraulic press

The DCB specimens were subjected to a 30 bar pressure for approximately 4 hours at 165º C. After curing, the spacers and the excess of adhesive were removed.

3.3.5 Removal and cleaning

After the curing time, cleaning and removing the excess of adhesive that remains was done outside the press. A knife and sandpaper were used to remove the excess of adhesive. Figure 38 presents the difference between specimens before and after cleaning.

Figure 38: Specimens cured and after cleaning.

3.3.6 Preparation for testing

After cleaning the excess of adhesive in DCB, the glue line must be visible. A coat of white tint was used for this purpose. A scale was attached to each specimen with the main purpose of controlling the crack length during the test (see Figure 39).

Figure 39: DCB specimen ready to be tested.

3.4 Determination of diffusion coefficient

3.4.1 Manufacturing of bulk specimens

An adhesive plate was machined with dimensions of 60 mm×60 mm and a thickness of 1 mm with the main propose of guarantying that water diffusions occur in just one dimension.

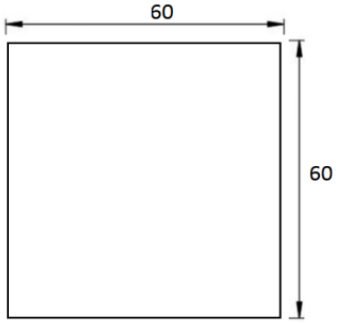

Figure 40: Bulk specimen (ISO 294-3) [39].

For this study, 3 specimens were prepared and before submerging in distilled water, they were placed in silicon dioxide during one week to dry and absorb any existing water in the bulk.

After dried, and before immersion in water, the specimens were abraded with sand paper. When the preparation was done, the specimens were immersed in distilled water at the temperature of 50 ˚C. This value was selected to provide a faster absorption of water and following the ISO62:2008, which propose a temperature 20 ˚C lower than T_g to avoid changes in the chemical properties of the adhesive.

Saldanha et al. [40] characterized the mechanical behavior of the epoxy adhesive Nagase Chemtex XNR6852 (Osaka, Japan), which is the first version of the adhesive studied in the present thesis. The T_g value obtained 102.6 ± 0.1 ºC. For that reason, it was assumed the value for the new version did not have a great variation.

During ageing, the bulk's weight was measured using a microbalance, with 1 mg of accuracy (Kern-Toledo, Balingen, Germany). This measurements were done until the mass of water uptake stabilized and reach a constant value, called infinite mass (M_∞).

3.4.2 Specimens ageing

Ageing the DCB specimens was carried out by immersing in deionized water at a temperature of 50 ºC. The specimens were placed in a way to ensure that all visible sides of the adhesive layer were in complete contact with water. They were kept in deionized water for 30 days.

3.4.3 Diffusion analysis

The moisture uptake was measured by analyzing the weight change before ageing and after immersion considering the time:

$$M_t = \frac{m_t - m_0}{m_0} \times 100\% \qquad \text{Eq. 21}$$

where M_t is the water uptake at any time, m_t is the mass of the specimen at any time t while ageing occurs and m_0 is the bulk' specimen mass when dried.

$$D = \pi \left(\frac{h}{4M_\infty}\right)^2 \left(\frac{M_T}{\sqrt{t}}\right)^2 \qquad \text{Eq. 22}$$

According to Ameli et al. [33] "toughened epoxy adhesives usually exhibit anomalous diffusion behavior in which a simple Fickian model tends to overestimate the water concentration at a given time". In this cases a dual Fickian must be considered to have a better correlation between analytical and experimental values.

The mass uptake for dual Fickian model at any time can be determined by:

$$M_T = \left(1 - \frac{8}{\pi^2}\sum_{n=0}^{\infty}\frac{1}{(2n+1)^2} e^{\frac{-D_1(2n+1)^2\pi^2 t}{4l^2}}\right) \times M_{1\infty} + \left(1 - \frac{8}{\pi^2}\sum_{n=0}^{\infty}\frac{1}{(2n+1)^2} e^{\frac{-D_2(2n+1)^2\pi^2 t}{4l^2}}\right) \times M_{2\infty} \qquad \text{Eq. 23}$$

where $M_{1\infty}$and $M_{2\infty}$ are the saturated masses and the sum of both provides the total saturated mass, $D_1$and D_2 are the diffusion coefficients and l is the diffusion path [41].

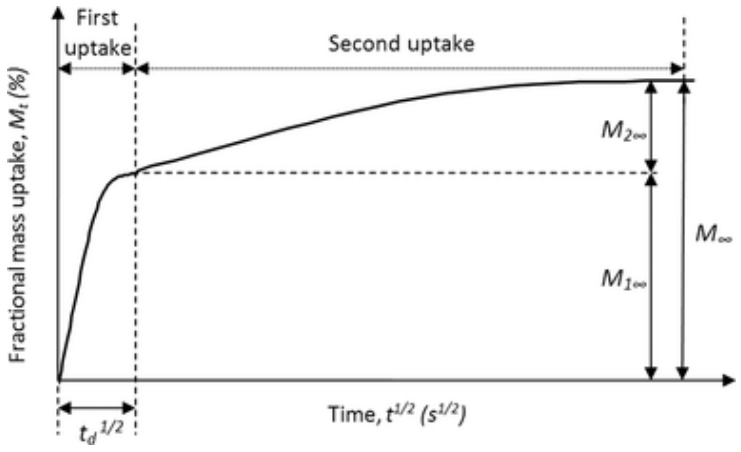

Figure 41: Schematic of the sequential dual Fickian model [34].

Figure 41 was used to identify the dependence of these parameters, in order to make the analytical model.

Figure 42 presents the experimental values for bulk specimens and the analytical vales for dual Fickian model. A good correlation between analytical and experimental values is observed. For that reason, two diffusion coefficients were measured assuming a non Fickian behavior. Diffusion coefficients and maximum absorption values (in percentage) are presented in Table 6.

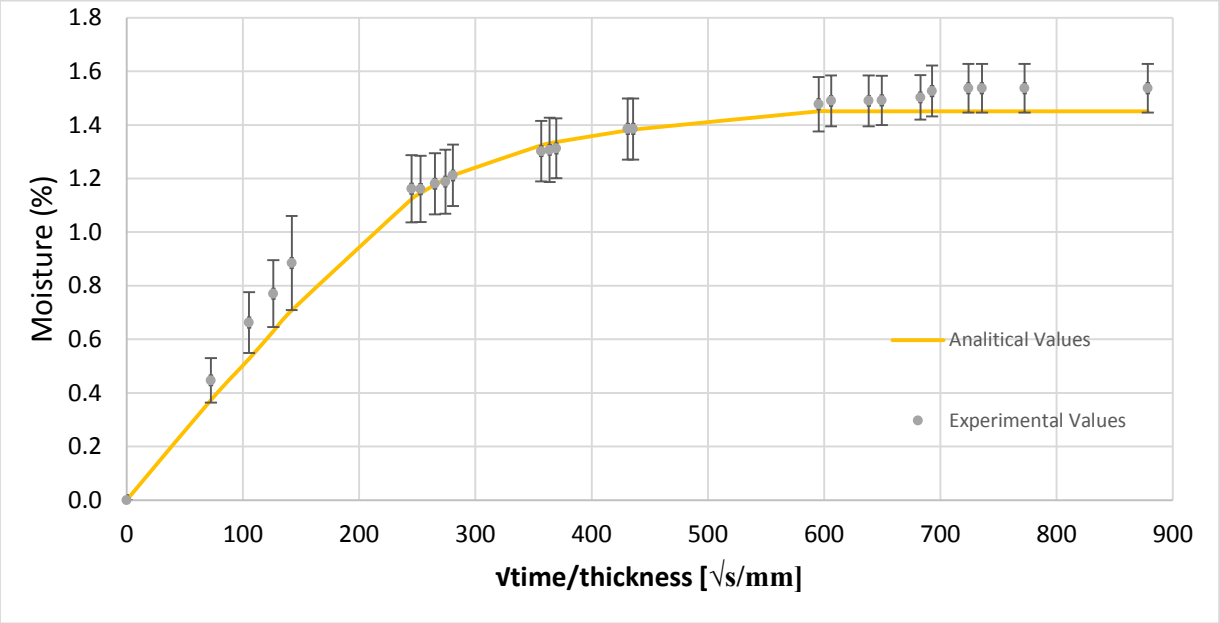

Figure 42: Analytical and experimental values of moisture as function of square root time.

The value of diffusion of specimens at 50 °C is higher than the values obtained at 30 ºC (as shown in Figure 43) which means the water molecules penetrate more quickly into the interior of the polymer chains [4].

Table 6: Coefficients of diffusion determined by curve fitting to experimental data for 50ºC.

	First behavior (D_1)	**Second behavior (D_2)**
Diffusion Coefficient	1.94×10^{-12} m^2/s	2.54×10^{-13} m^2/s
Maximum absorption	1.17%	0.35%

Figure 43 presents an evaluation of percent (%) mass growth as function of square root time for two temperatures. Both curves show a similar value for the maximum value of water uptake. For 50 ºC, the first slope is higher than for 30 ºC. Dual Fick behavior is observed for both

temperatures. D_1 and D_2 are the diffusion coefficients of the first and second moisture uptake mechanisms, respectively.

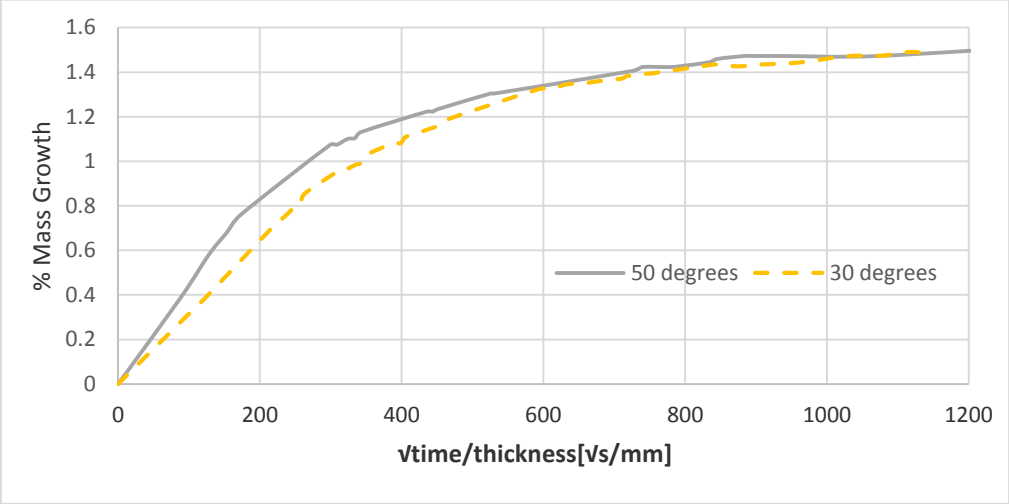

Figure 43: Mass growth for two temperatures.

3.4.4 Swelling measurement

Swelling is a volumetric variation accompanying the moisture diffusion in a thermosetting epoxy system [26]. This phenomena can also increase when the temperature increases as a consequence of the growth of maximum water uptake. Swelling of the adhesive can have an important effect on adhesive joint durability as it can induce significant strain.[26].

The thickness variation was controlled recurring to a micrometer (Mitutoyo, Mizonokuchi, Japan) and consequently swelling was measured following:

$$\frac{\Delta V}{V_0} = \frac{V_f - V_0}{V_0} \qquad \text{Eq. 24}$$

where V_f is the volume of the bulk specimen after aging and V_0 is the volume after drying and before aging. During the aging, the thickness in three different points did not change, so no swelling was verified in this adhesive with the temperature of 50 ˚C.

3.5 FTIR analysis

The results obtained in the Fourier transform infrared spectroscopy (FTIR) analysis demonstrated that the presence of water can modify the properties of the studied.materials. This analysis were carried out by use of a PerkinElmer Spectrum Two apparatus (Waltham, USA) [4]. It is necessary to analyse whether these differences are also visible at the level of the

chemical structure. In order to understand that phenomena, the dry and aged epoxy was analysed by FTIR.

FTIR spectra helps to recognize the effects of water uptake, given that irreversible damage occurs, the intensity of absorption bands for relevant groups will change. Wave lengths of (4000–600) cm^{-1} and 0.2 cm^{-1} of scanning velocity were used. These tests were carried out with a LiTaO3 detector (15,700–370 cm^{-1}) and a KBr window. The Spectrum 10 PerkinElmer software Spectrum (Waltham, USA) was used for the data analyses [4]. Two bulk specimens were used to compare the dry and saturated conditions (approximatly 1 mm thickness).

3.6 Fracture tests

According to Wylde and Spelt "the strength of a wide variety of joint geometries can be predicted using the 'fracture envelope' of an adhesive system" [31]. In order to obtain the fracture envelope, pure mode I, pure mode II and mixed-mode tests have to be performed.

3.6.1 Mode I tests (DCB)

The determination of G_{IC} was done recurring to DCB tests. This test consists in solicitation of the adhesive for an opening mode. Three specimens were tested. During the tests, the values of the load and the displacements were recorded by the computer data acquisition using an Instron 3367 Universal Testing Machine (Norwood, USA) with a load cell of 30 kN. The R-curves were obtained using the CBBM.

Before beginning the tests a pre-cracking was done for all specimens with the main propose of avoiding a blunt crack. The pre-crack is an important step since the edge of the blade presents a curvature radius that will cause an energy increase needed for the propagation of the crack. After this, a_0 was measured. The tests were performed at room temperature and at a constant displacement rate of 0.1 mm/min.

Figure 44: Execution of the mode I test.

Data analysis

The data reduction was made recurring to the CBBM [42], which depends only on the specimen's compliance during the test. G_{Ic} can be obtained with following expression:

$$G_{Ic} = \frac{6P^2}{b^2h^3}\left(\frac{2a_e^2}{E_f} + \frac{h^2}{5G}\right) \quad \text{Eq. 25}$$

where E_f is the corrected flexural modulus, G is the shear modulus of the adherends and a_e is the equivalent crack length and it is given by:

$$a_{eq} = a + |\Delta| + \Delta a_{FPZ} \quad \text{Eq. 26}$$

This value takes into consideration the FPZ at the crack tip. Δ is the root rotation correction for the initial crack length obtained from the linear regression of $C^{1/3}$=f(a_0).

3.6.2 Mode II tests (ENF)

The geometry used for the ENF test specimen is the same that was used for the mode I test (Figure 33). The tests were performed at room temperature and at constant displacement rate of 0.2 mm/min. A Teflon® film with oil droplet was introduce in the initial part of the ENF specimen to provide an initial crack length without friction.

.In order to avoid the effect of blunt crack and ensure the right propagation of the crack, the specimens were lightly loaded in opening mode before starting the tests. Then, the initial crack length, a_0 was measured.

Figure 45: Execution of the mode II test.

The CBBM was used to obtain the G_{IIc} recurring to:

$$G_{IIc} = \frac{9P_{II}^2 a_{eII}^2}{16b^2E_f h^3} \quad \text{Eq. 27}$$

The CBBM is particularly important in the ENF test because the crack length monitoring during its growth presents some difficulties. For that reason, the concept of equivalent crack length is important to avoid the measure of crack length during the test.

3.6.3 Mixed-mode tests

The mixed-mode tests were performed using a test apparatus (portuguese patent nº 107188 B). The purpose of the loading jig is to perform mixed-mode fracture testing of adhesively bonded DCB joint specimens over a varied range of mode combinations from pure mode I to pure mode II. This apparatus allows the fracture envelope to be measured using a DCB specimen. Adjusting the pin locations allows fracture toughness to be measured over the entire range of mode ratios from pure mode I (φ=0°) to near pure mode II (φ=90°) and nominal phase angle of loading, φ can be obtained by:

$$\varphi = arctan\left(\frac{\sqrt{3}\left(\frac{F_1}{F_2}+1\right)}{2\left(\frac{F_1}{F_2}-1\right)}\right) \quad \text{Eq. 28}$$

where F_1 and F_2 are the loads shown in Figure 47.

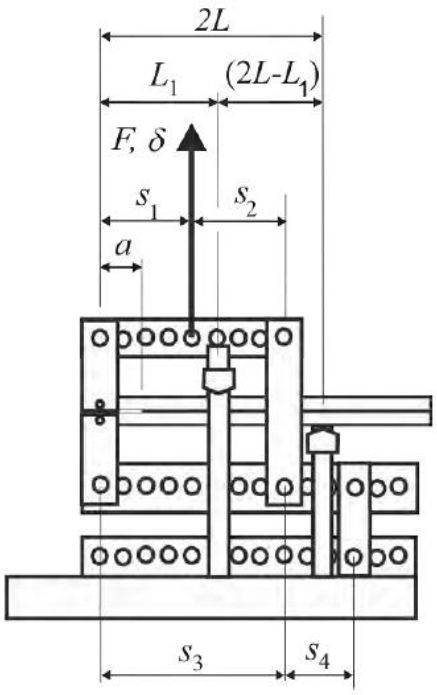

Figure 46: Mixed-Mode apparatus schematics [5].

Data analysis

The method of calculation is the CBBM [21]. To perform test between mode I and mode II some inputs are necessary:

1. A **load *F*** was obtained from an Instron 3367 Universal Testing Machine (Norwood, Usa) with a capacity of 30 kN;
2. Displacements ***δ₁* and *δ₂***, obtained from LVDTs attached to each beam;
3. Geometry and material properties **(*B, h, E, G*)**: different jig geometries can be achieved by altering the four distances, **s_1 - s_4**, thereby varying the mode ratio.

The loads and displacements components can be obtained as shown in Figure 47.

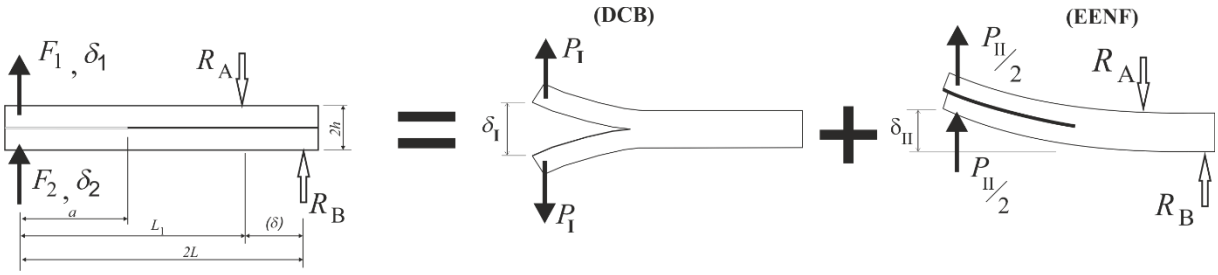

$$F_1 = F\frac{s_2}{s_3} \quad ; \quad F_2 = F\frac{s_1 s_4}{s_3\left(s_3+s_4\right)} \qquad P_I = \frac{F_1 - F_2}{2} \qquad P_{II} = F_1 + F_2$$

$$\delta_I = \delta_1 - \delta_2 \qquad \delta_{II} = \frac{\delta_1 + \delta_2}{2}$$

Figure 47: Jig loading scheme with mode I and mode II partition [5].

Mode I and II compliances have to be obtained from:

$$C_I = \frac{\delta_I}{P_I} = \frac{3a^3}{Bh^3E} + \frac{12a}{5BhG}$$

$$C_{II} = \frac{\delta_{II}}{P_{II}} = \frac{3a^3 + 2LL_1^2}{2Bh^3E} + \frac{6LL_1}{5BhG(2L - L_1)} \qquad \text{Eq. 29}$$

Fracture toughness for mode I is given by:

$$G_I = \frac{6P_I^2}{b^2h^3}\left(\frac{2a_{eI}^2}{E} + \frac{h^2}{5G}\right) \qquad \text{Eq. 30}$$

For mode II comes from:

$$G_{II} = \frac{9P_{II}^2 a_{eII}^2}{16b^2Eh^3} \qquad \text{Eq. 31}$$

4 Numerical modelling

4.1 Moisture concentration distribution

The 2D finite element (FE) model was built in ABAQUS®. To model moisture diffusion in FEM (finite element modelling), an analogy between heat transfer and moisture diffusion can be used [22]. According to da Silva et. al [14], "when salt is dissolved in water, in effect it dilutes the water, and the amount of water which is absorbed is reduced." For that reason, simulations were made using the values of distilled water, with the main purpose of predicting the area affected by the moisture as a function of time.

Figure 48 represents the adhesive layer in DCB specimens and the blue section corresponds to the part used for modelling in ABAQUS®. This section was chosen considering the symmetry of the adhesive layer and boundary conditions.

Figure 48: Schematic of the adhesive in a DCB' specimen and the symmetry used for modelling

The dimension of this problem is:

Number of elements	40000
Number of nodes	40401

In order to predict the state of environmental degradation in an adhesive system, the values used are present in Table 6. The values for each behavior were modelled in ABAQUS® with 4- node linear solid finite element (DC2D4).

4.2 Fracture tests

Numerical models implemented in ABAQUS® using cohesive elements defined with subroutines were used to validate experimental results with DCB specimens' geometry. The specimen's beams were modelled with plane-strain 8-node quadrilateral solid finite elements (CPE8R from ABAQUS®) and the adhesive was modelled with 6-node cohesive elements [43]. The mechanical and cohesive properties used in the simulations are shown in Table 7.

Table 7: Elastic and cohesive properties.

Elastic Properties (Aluminum)		Cohesive Properties (Adhesive: Nagase Chemtex XNR9852-2)			
E [GPa]	G [GPa]	G_{Ic}[N/mm]	G_{IIc}[N/mm]	$\delta 2_{,I}$ [mm]	$\delta 2_{,II}$ [mm]
70	27	1.6	17	0.035	0.65

4.2.1 Mode I

The dimension of this problem is:

Number of elements	4080
Number of nodes	12514
Total number of variables in the model	25028
Cohesive elements	240

Trapezoidal cohesive laws are appropriated when ductile adhesives are used, to provide the influence of plasticity. The trapezoidal softening law replicates with accuracy the behavior of thin adhesive layers [43]. Figure 49 represents the trapezoidal law used to characterize the adhesive in pure mode I with a 0.2 mm adhesive thickness. The graph represents three different stages of the cohesive law:

- Elastic deformation is represented for the first slope of σ-δ;
- The plateau represents the plastic behavior of the adhesive;
- The third stage is the final rupture.

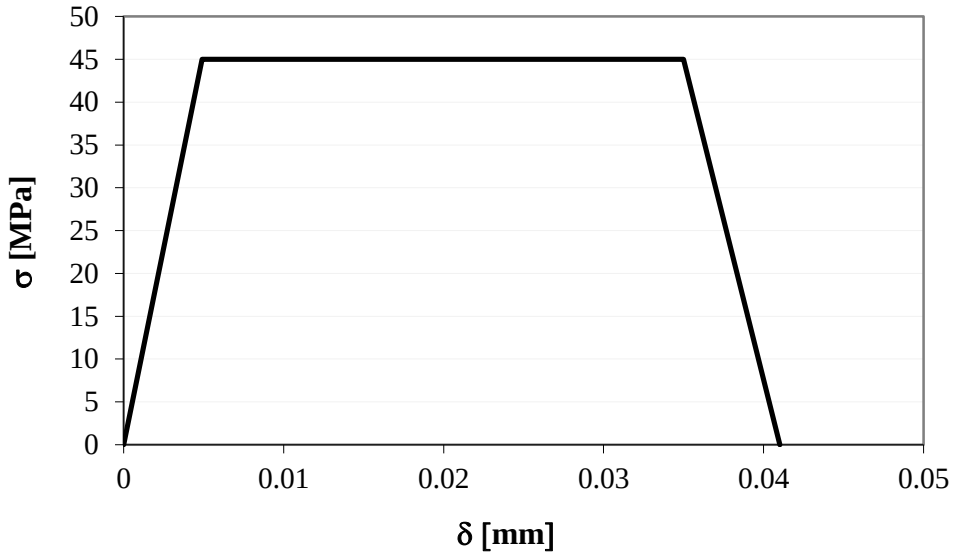

Figure 49: Trapezoidal softening law for pure cohesive damage model for mode I.

4.2.2 Mode II

The dimension of this problem is:

Number of elements	2245
Number of nodes	7077
Total number of variables in the model	13493
Cohesive elements	311

A numerical analysis was performed to characterize the trapezoidal cohesive law in pure mode II with a thickness of 0.2 mm. Figure 50 characterizes the trapezoidal softening law for pure mode II. The $\sigma_{u,II}$ has a value of 22.8 MPa.

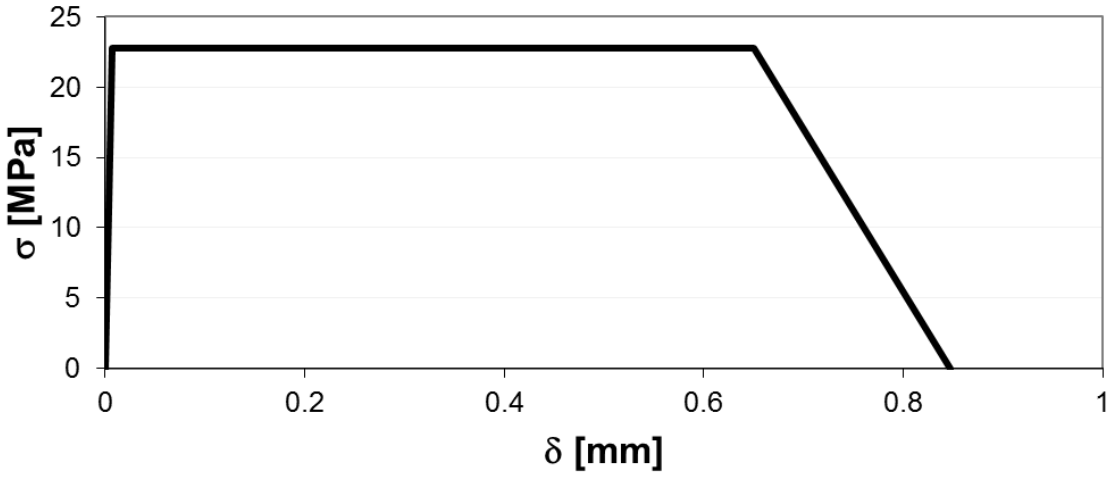

Figure 50: Trapezoidal softening law for pure cohesive damage model for mode II.

5 Results and discussion

5.1 Diffusion analysis

5.1.1 FTIR

Figure 51 shows the spectrum in the 4000-450 cm^{-1} wavenumber range of Nagase XNR 6852E-2. This figure shows the two states of moisture studied in this research: dry and after one month ageing (30 days) at 50 ºC (using a bulk specimen).

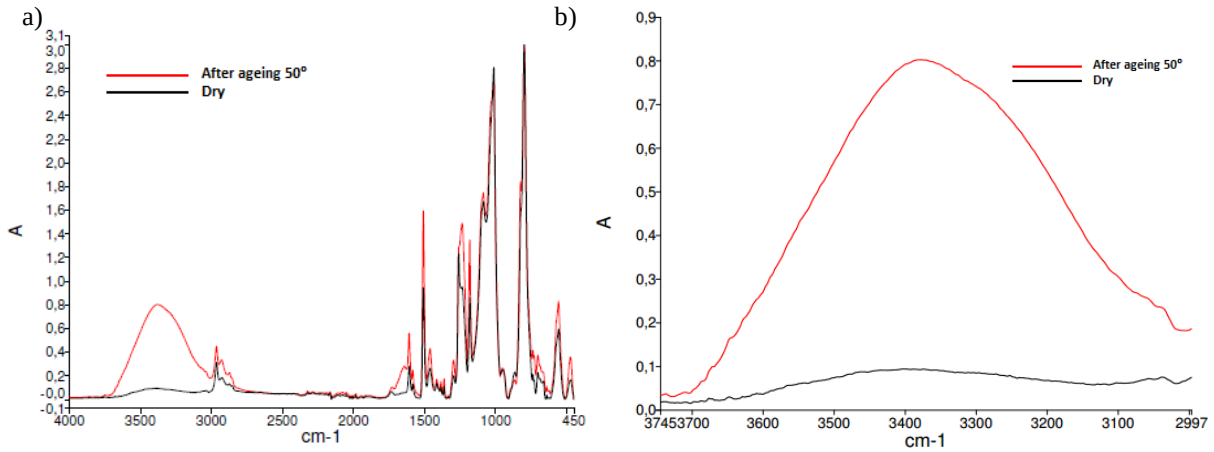

Figure 51: FTIR spectrum: (a) in the 4000-450 cm^{-1} wavenumber range of neat resin for different stages of moisture (dry and aged one month at 50º C) (b) in the 4000-3000 cm^{-1} wavenumber range (-OH group).

A general data analysis leads to the conclusion that the spectra has a similar behavior (Figure 52). Exploring the spectrum for the different points some differences can be observed. The –OH $–CH_2$ and C–N groups increase with aged conditions (3378 cm^{-1}) compared with dry conditions [4].

After aging in water at 50 ºC, there is an increase of the –OH group, as this absorption is due to O–H and N–H stretching and intermolecular hydrogen bonds; this can be explained by the fact that water absorption induces hydroxyl and amine groups into the epoxy chain. It is also observed that C–H stretching vibrations (3100–2800 cm^{-1}) increased, arising from aliphatic hydrocarbons, which also changes with the water absorption [4, 44, 45].

Changes were observed in C=C streching of the benzene ring and the out-of-plane bending of aromatic rings (1507 cm^{-1}) and out- of- plane bending of aromatic rings (823 cm^{-1}). The aromatic band (1234 cm^{-1}) increases when bonded water is present. All these mentioned changes confirms that there is water absorption by the epoxy resin [4].

The analysis of the functional groups present in both types of samples shows that there are changes (especially in the –OH group) along the two stages (dry and wet).

Selected points in Figure 52 correspond to strategic points in the adhesive layer. It is relevant to notice the water distribution along the DCB specimen.

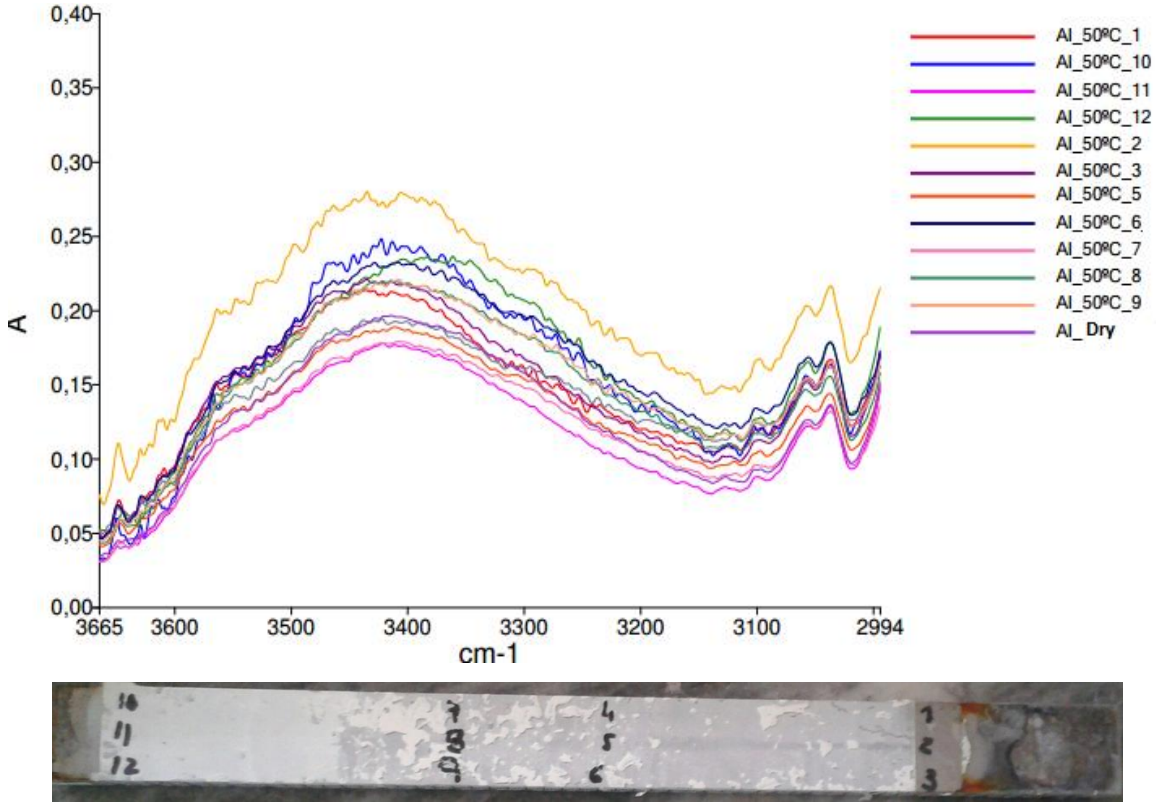

Figure 52:-OH group spectrum for different points in DCB specimen.

Analysing the spectrum of the Figure 52, the observed that the –OH peak is higher for the point in the middle of the blade. The distributution of the 12 points along the adhesive layer was selected having in concern strategic points of water uptake. This means different distances to the boundary where the moisture content has an expected maximum value.

This interval was selected to evaluate the water's influence, which is more noticeable at the peak of the –OH. Compared to the saturated bulk specimen where the saturation level is approximately 0.8, the highest values are between 0.15 and 0.3 for which it can be concluded that these points are far from saturation.

5.1.2 Numerical modelling

Figure 53 and Figure 54 show the distribution of water uptake after 4 weeks ageing (real time ageing) for first and second Fick, respectively. Higher values can be observed closer to the boundary. The closer to the center of the specimen, the less is the concentration of water until the center where it is insignificant. Therefore it is possible to obtain the differences between diffusion coefficients. These figures have the same time frame, which means they were studied

at the same point in time, however the distribution along adhesive layer has significant differences.

The first Fick behavior, represented in Figure 53, shows that the distribution of water is considerably larger than in the second Fick (Figure 54). This means that second Fick has a lower influence in aging when compared with first Fick.

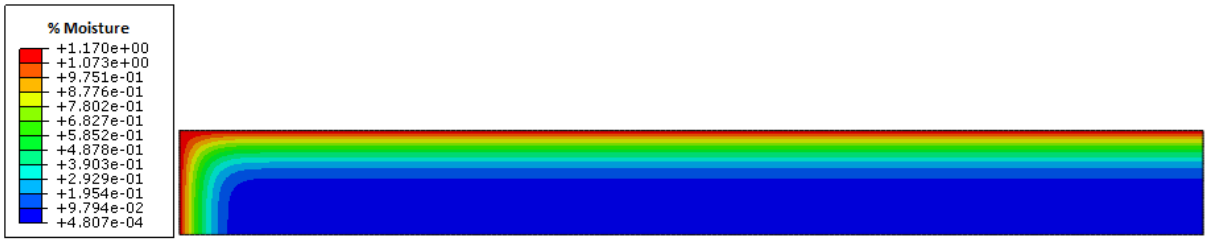

Figure 53: Simulated water uptake after one month ageing (¼ of the 25x245mm section of the DCB)-First Fick.

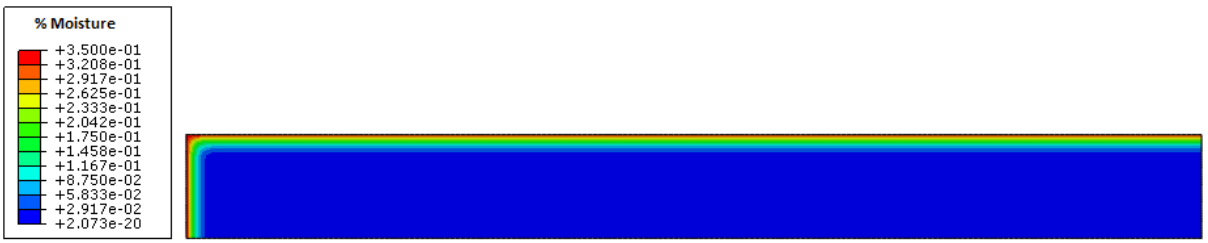

Figure 54: Simulated water uptake after one month ageing (¼ of the 25x245mm section of the DCB)-Second Fick.

The evolution of water uptake along the DCB width is shown in Figure 55. Two dates were modelled with the main purpose of comparing the behavior of moisture evolution along the DCB width. The curve tends to go up as time passes.

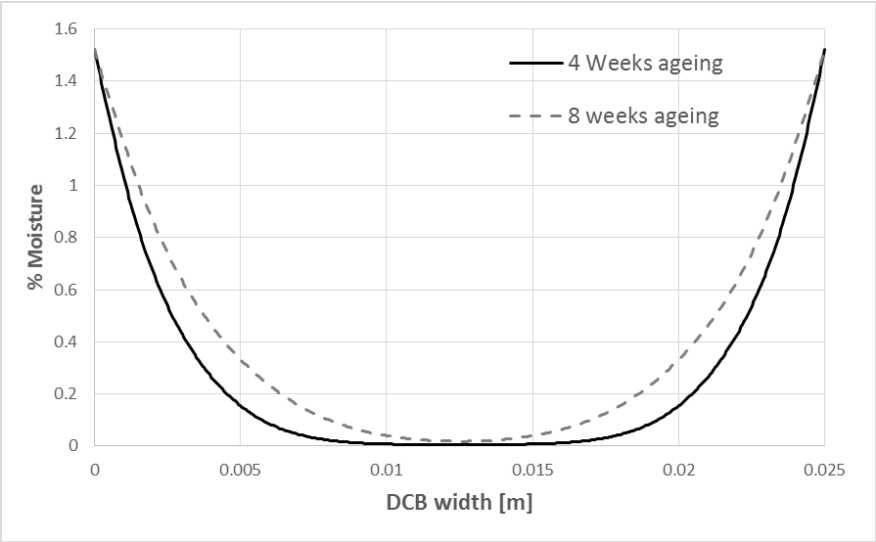

Figure 55: Percentage of moisture along the DCB width (distance along the joint) with 4 and 8 weeks ageing.

Three points from the mesh were selected. The main objective is to understand which points get to the saturation point faster and the time needed to obtain a significant level of saturation.

According to Figure 56, points closer to the boundary have a faster saturation when compared with points in the middle of the adhesive layer. This figure shows the difficulty of obtaining complete saturation of DCB specimens. For the points closer to the boundary, two weeks are needed to get to saturation level.

The specimens spent one month ageing which corresponds to approximately 1610 $\sqrt{s}/mm$. At this time, the percentage of moisture for point E is 1.41%, for point M is 1.05% and for point I is 0.1%. The difference in these values is attributed to the distance from the boundary and consequently the distance from the distilled water.

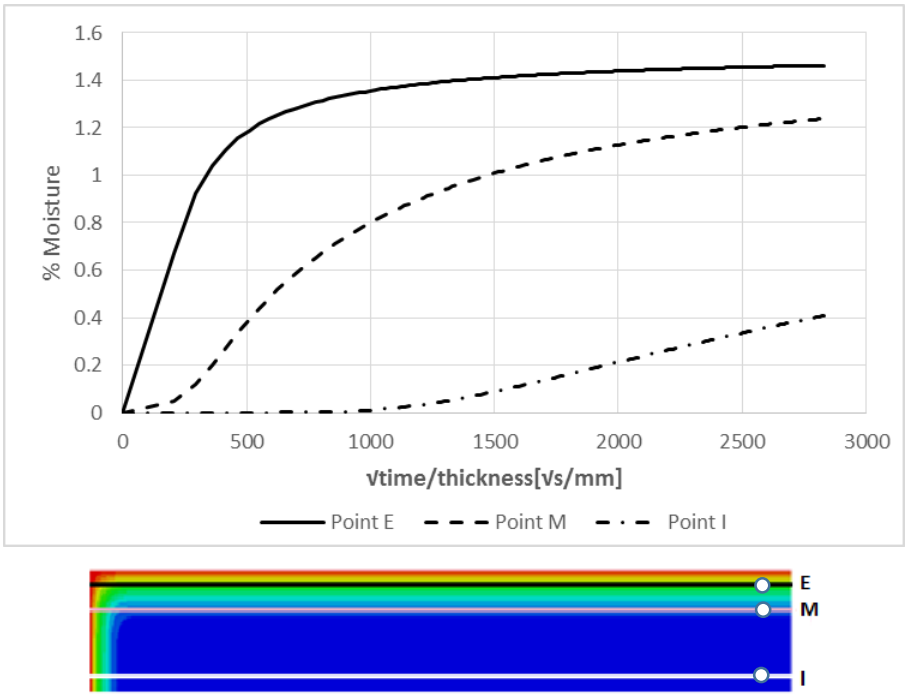

Figure 56: Prediction of percentage of water uptake as function of time.

Numerical modelling vs. FTIR analyses

The FEA and FTIR analysis are important tools to provide information about the moisture content in adhesive layer in DCB specimes. The main purpose of these studies is to find an agreement in results and validate the numerical modelling.

As mentioned before, the FTIR provides qualitative information about the water distribution along the adhesive layer (see Figure 52).

An important step in this analyses is to compare with numerical model results presented in Figure 53 in Section 5.1.2. The information provided for Figure 52 is in good agreement with numerical simulation. Both analysis show a maximum of water content in the boundary line and a decrease when closer to the middle of DCB width.

5.2 Mode I

The DCB's tests were used to obtain the fracture toughness for mode I, G_{Ic}. The aluminum adherends did not experience any plastic deformation. Cohesive failure was observed for all the tested specimens.

5.2.1 Dry

Nagase XNR 6852E-2 was tested for mode I using three aluminum 7075 specimens. As can be observed in Figure 57, the failure in the DCB specimens was cohesive. The displacement rate was 0.1 mm/min to provide a stabilized crack growth.

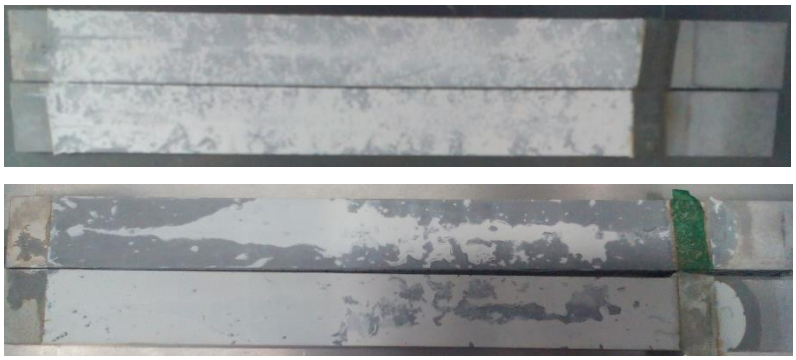

Figure 57: Failure surface of a DCB specimen in mode I (dry conditions).

P-δ curves obtained from DCB tests are shown in Figure 58. Initially, the applied load increases, the stored elastic energy increases until the stored energy equals the energy required to begin the spread of the crack, G_{Ic}. The initiation of the crack propagation is characterized by a decrease in the applied load. Each curve's peak represents the critical load. The first curve presents a higher value than the other ones probably due to a presence of adhesive in the blade.

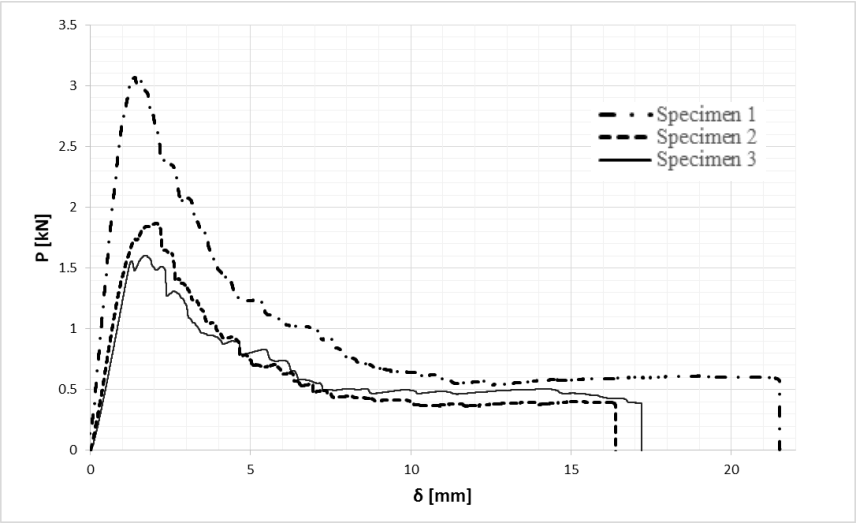

Figure 58: *P-δ* curve for three tests in mode I (dry specimens).

The CBBM was used to get the R-Curves [5]. These curves provide the critical strain energy release rate, G_{Ic}, which initially increases with crack length [33]. As the crack progresses, the G_{Ic} value converges to a plateau that gives the fracture toughness, and in most cases stabilizes in that level [18].

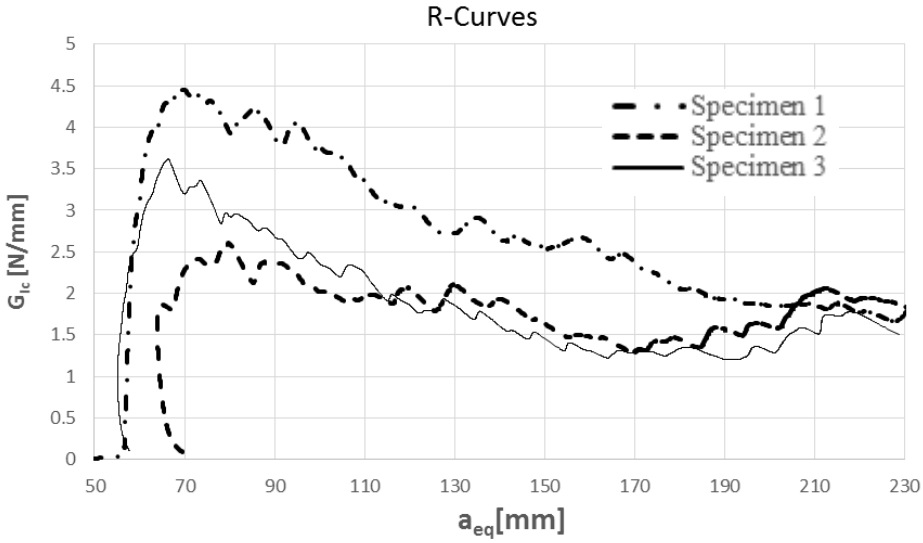

Figure 59: Experimental R-curve obtained for the DCB test using CBBM.

P-δ curves and R-curves provide the values of critical loads and fracture toughness in dry conditions (see Table 8). The average value acquired for fracture toughness for mode I loading was 1.5 N/mm. This value is in accordance with the values obtained with a different adherend material, high grade steel, shown in Appendix A.

Table 8: Values obtained for mode I-dry conditions.

	1	2	3	Average
Max. load [kN]	3	1.8	1.6	1.8±0.8
G_{Ic} [N/mm]	1.8	1.5	1.3	1.5±0.25

5.2.1.1 Numerical results

Numerical simulation provides the stresses distribution along the adherends (see Figure 60). The maximum stress obtained in the simulation was 122 MPa and according to the material's properties defined in Section 3.1, substrates does not experience any plastic deformation (Al7075 yield strength is 455 MPa). A more refined mesh is used in the damage propagation zone, near the adhesive layer [43].

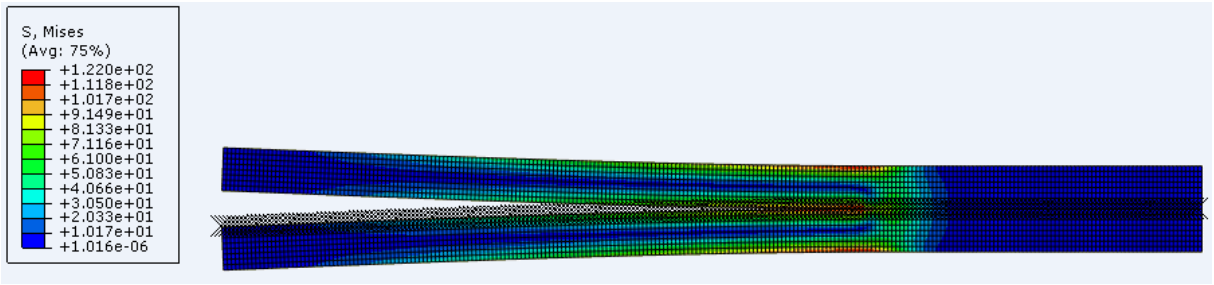

Figure 60: Deformed-shape for mode I loading.

Numerical and experimental values for *P-δ* curves are shown in Figure 61. The numerical curve is in good agreement with the experimental result.

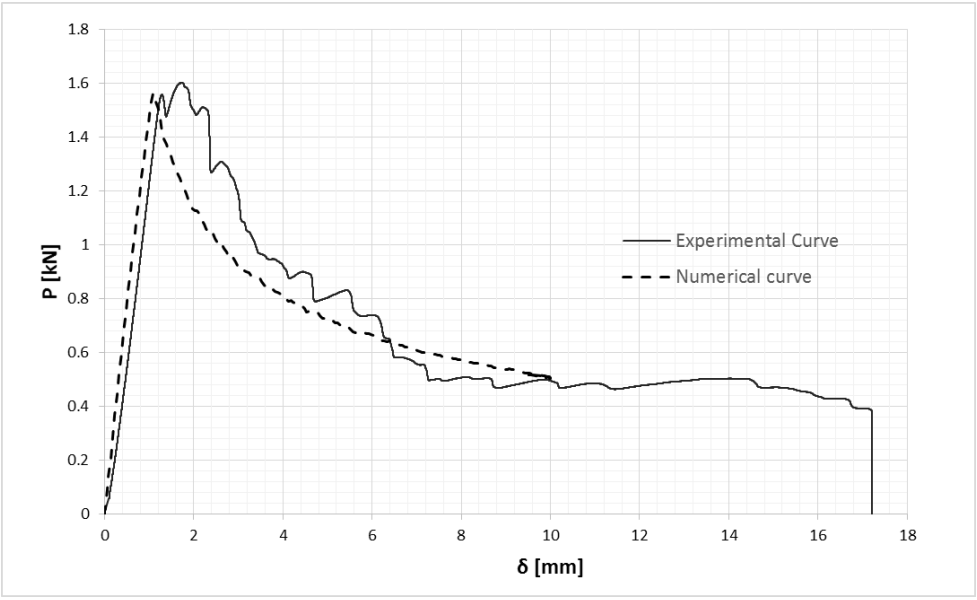

Figure 61: Numerical and experimental *P-δ* curves for mode I loading

5.2.2 Wet ageing

After one month ageing, three specimens were tested to characterize the adhesive toughness in mode I with a displacement rate of 0.1 mm/min. The testing conditions were the same used for dry conditions with the main purpose of comparing only the influence of moisture in the results. *P-δ* curves for dry and wet conditions are present in Figure 62.

The results observed in the *P-δ* curves show an increase in displacement after ageing in distilled water from 15 to 20 mm, approximately.

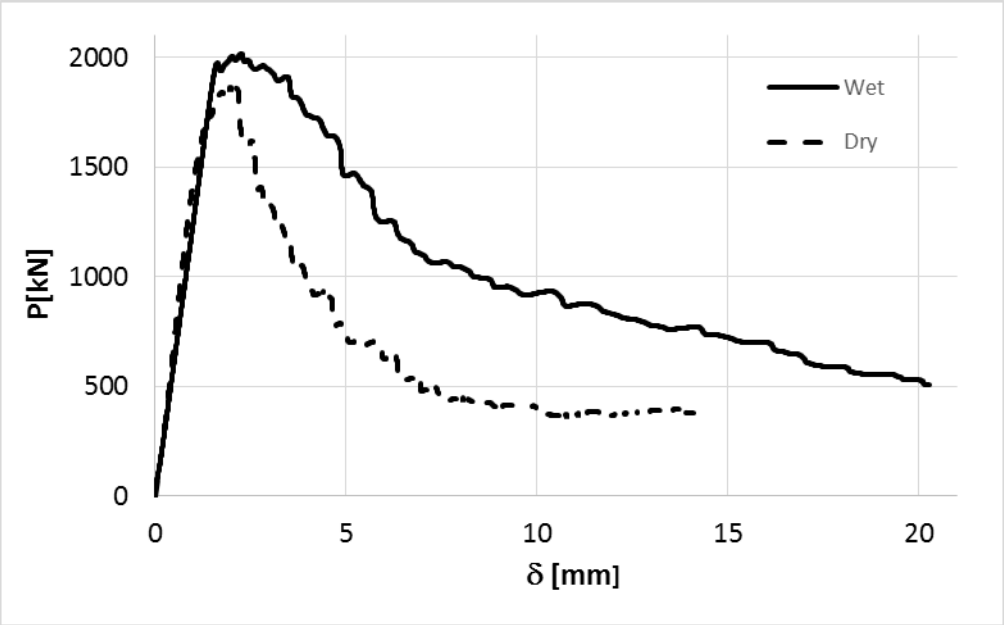

Figure 62: *P-δ* curve for DCB test dry and wet conditions.

The critical value for fracture toughness in mode I increases from 1.5 to 3.86 N/mm. The average value required for fracture toughness for mode I loading after one month ageing was 3.86 N/mm, as shown in Table 9. This value is in accordance with Wyld and Spelt study about an epoxy system verifying an increase of fracture toughness after 30 days ageing (Figure 25). According to the authors, the increase of plasticization is not important with degradation evolution [31].

Table 9: Fracture toughness values obtained for mode I-wet conditions.

	1	**2**	**3**	**Average**
G_{Ic} **[N/mm]**	4.152	3.896	3.53	3.86±0.31

The R-curves for both *P- δ* curves are presented in Figure 63. The R-curve behavior is quite similar, however a decrease in the plateau is evident after ageing in distilled water. The

increasing value in wet specimens can be associated with the "blunt" effect, as shown in Figure 57, the curvatures of the blade can change the results and increase the "real" value [18].

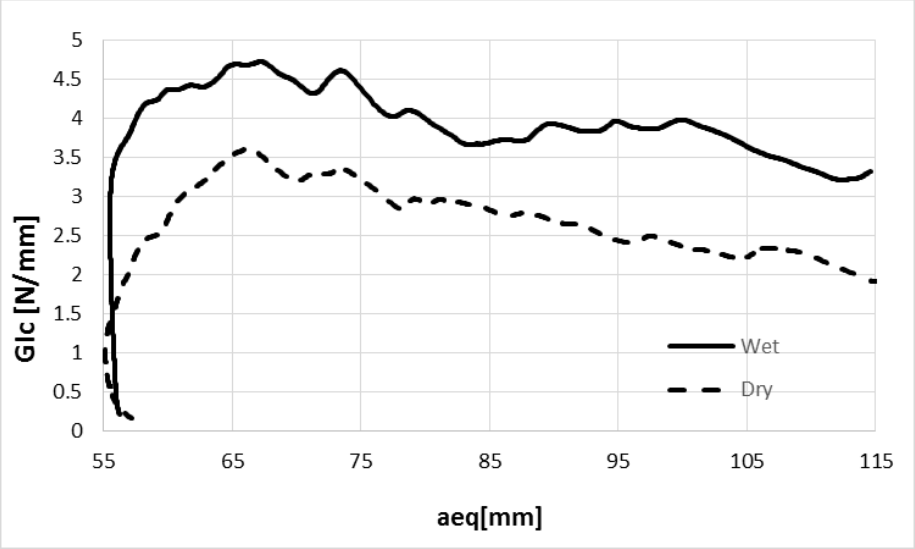

Figure 63: R-Curves for DCB tests in dry and wet condition for mode I.

5.3 Mode II

The ENF test was used to characterize in pure mode II a 0.2 mm thick adhesive layer of Nagase Chemtex® XNR 6852E-2. To perform the ENF tests, the experimental setup is changed to allow testing a simply supported beam with a load in the middle of its length.

5.3.1 Dry

The Nagase XNR 6852E-2 adhesive was tested for mode II using three aluminum 7075 specimens. All the specimens failed cohesively in the adhesive. *P-δ* curves obtained from ENF tests are shown in Figure 64. The curve's behavior is non-linear corresponding to plastic deformation. The maximum load obtained in the first test was approximately 15 kN with a displacement of 5 mm. The highest value of critical load and the correspondent displacement represents the beginning of the stable crack propagation.

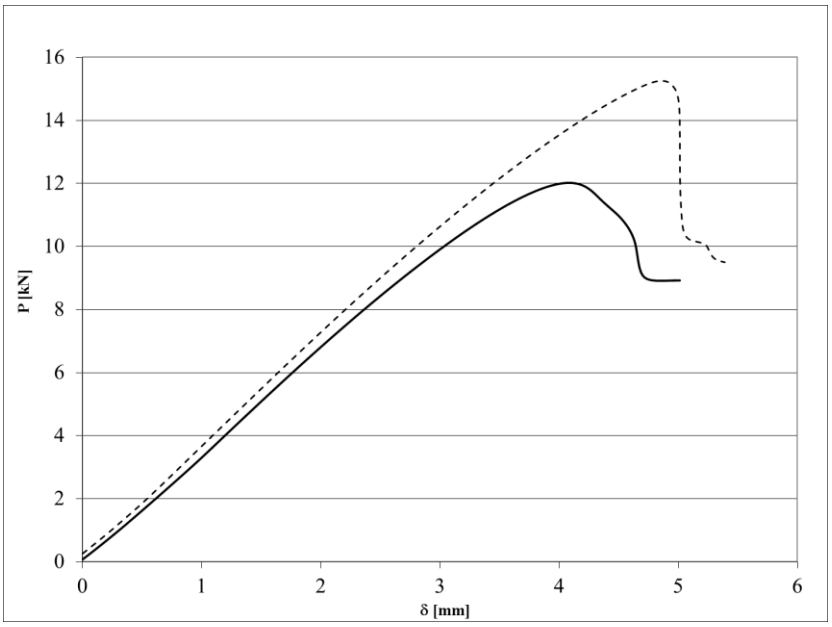

Figure 64: P- δ curves for ENF test dry conditions.

Table 10: Values obtained for mode II-dry conditions.

	1	**2**	**3**	**Average**
Max. load [N]	15103	14300	12000	13800±1315
***G*$_{IIc}$ [N/mm]**	14.923	12.83	10.52	12.76±2.20

The experimental R-curve obtained using he CBBM is shown in Figure 65. It is possible to recognize a plateau indicating a stable crack propagation for both curves. The average fracture toughness for pure shear mode was 12.76 N/mm.

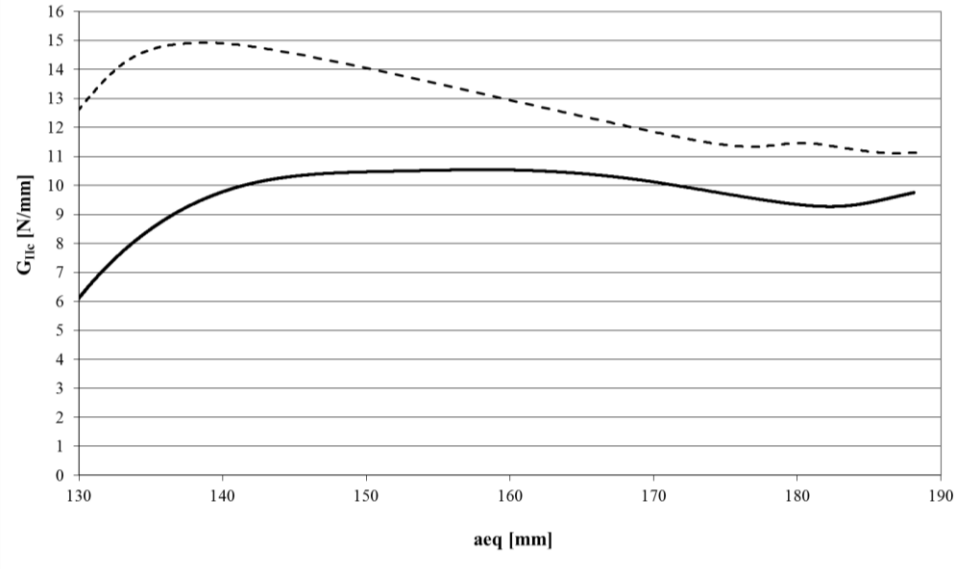

Figure 65: R-curves for mode II-dry conditions.

5.3.1.1 Numerical results

The maximum stress obtained in the simulation was 341 MPa and according with the material properties, the substrate does not experience plastic deformation (see Figure 66).

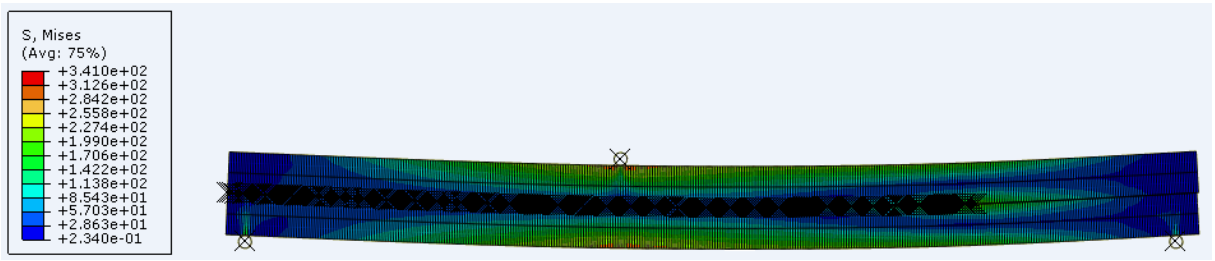

Figure 66: Deformed-shape for mode II loading.

Numerical and experimental values for *P-δ* curves are shown in Figure 67. The *P-δ* curves show a good correlation between experimental and numerical values.

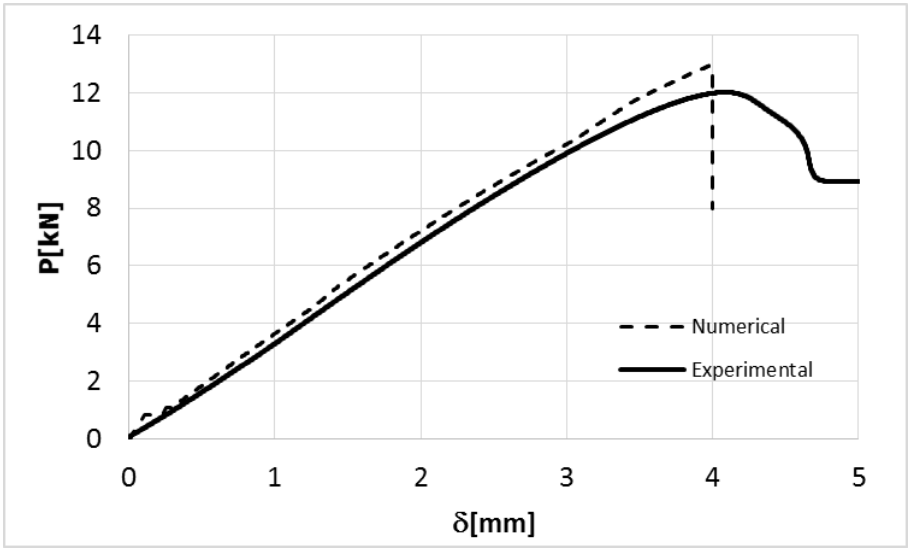

Figure 67: Numerical and experimental *P-δ* curves for mode II loading.

5.3.2 Wet ageing

The influence of water uptake for pure mode II has been studied. The specimens were taken from water when they were tested to avoid desorption of water.

Figure 68 compares two *P-δ* curves for dry and aged conditions. The *P-δ* curve increases until a maximum load, where the propagation of the crack begins. At that moment the load decreases because the crack has reached the necessary energy, $G_{IIc,}$ to initiate a stable propagation. After one month ageing, the fracture surfaces for all specimens were cohesive, as shown in Figure 69.

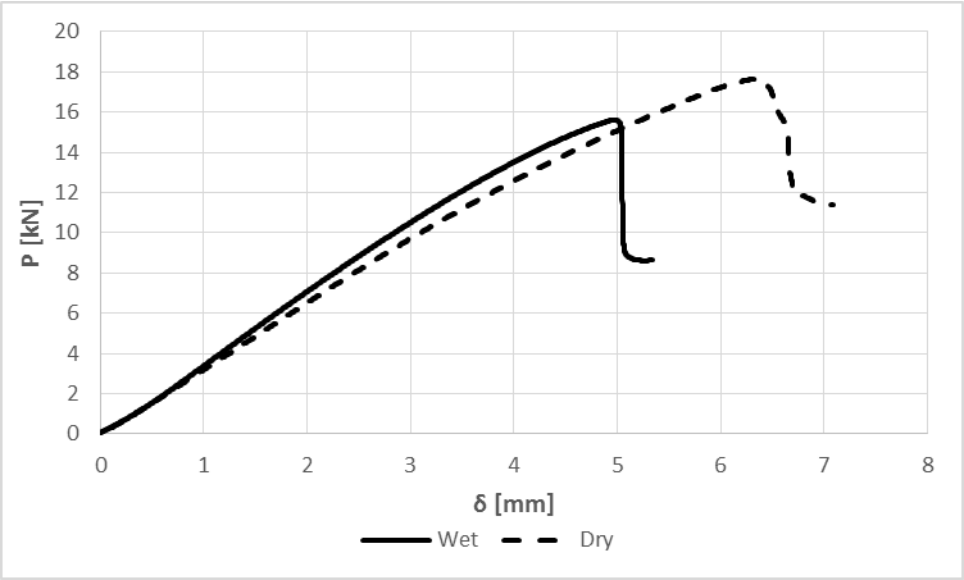

Figure 68: *P-δ* curve for ENF test dry and wet conditions.

Figure 69: Fracture surface for specimens after one month ageing.

The CBBM [42] was the method used to analyze the numerical data. This methodology overcomes the difficulty related with crack length measurement during the ENF test and takes into account the effect of the fracture process zone, relevant for ductile adhesives [46].

The R-Curve is presented in Figure 70. In this figure, it is possible to observe a plateau which corresponds to the critical energy release rate for each condition. The plateau descends after degradation.

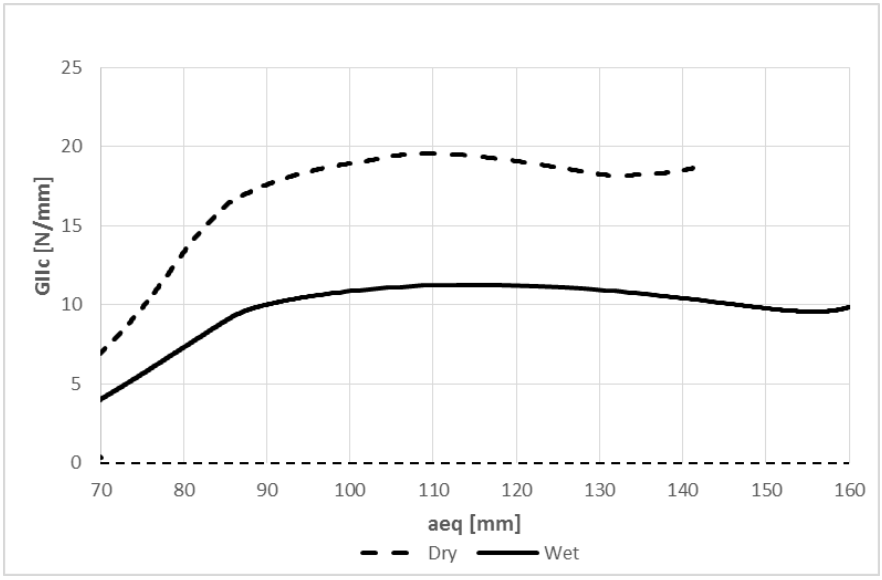

Figure 70: R-curves for mode II, wet and dry conditions.

From each R-curve, a plateau is selected which provides the G_{IIc}. The results are presented in Table 11.

Table 11: Values obtained for mode II-wet conditions.

	1	**2**	**3**	**Average**
G_{IIc} **[N/mm]**	11.27	11.73	12.50	11.73±0.51

5.4 Mixed-mode

Understanding the crack propagation behavior under realistic types of combined (opening and shear stress components) service loading is an important aspect of evaluating the performance of an adhesive joint. The mixed mode apparatus provides a test which applies mode I and mode II loads to a DCB specimen while measuring the displacement of each beam and applied load, allowing to measure its fracture toughness for each mode.

5.4.1 Phase angle: φ= 11.25º

The s_1-s_4 dimensions are described in Table 12. The nominal phase angle of loading, φ, for this case is 11.25º.

Before performing the tests in mixed mode, the joint was slightly pre-loaded (0.1 mm/min).

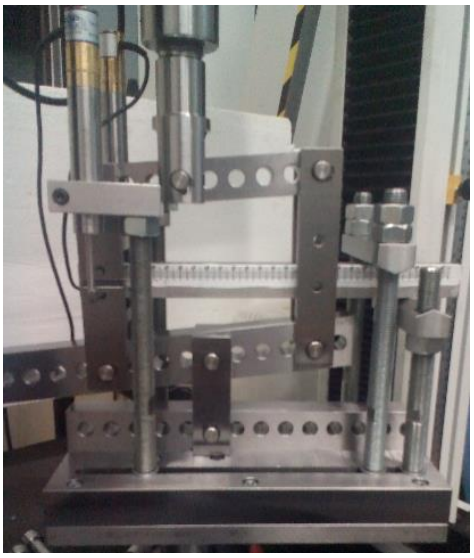

Figure 71: Apparatus with s1-s4 combination for φ=11.25º.

Table 12: s1-s4 combination for φ=11.25º.

S1	S2	S3	S4
60	100	160	-80

5.4.1.1 Dry

The load - displacement (*P-δ*) curve and the specimen's beams' displacements (δ_1 and δ_2) recorded by the LVDT's are presented in Figure 72. The *P- δ* curve is supposed to begin with a load and zero displacement, however the test needs an initial load to eliminate gaps. The data acquisition begins with almost 1 kN which corresponds to the load necessary to eliminate any slack in the system

The final distance between beams was 22 mm. For a pure mode I, it is supposed to obtain symmetric displacement curves provided by the LVDTs, but in this case, some contribution of mode II is represented by the "asymmetry" in displacements δ_1 and δ_2 during the test.

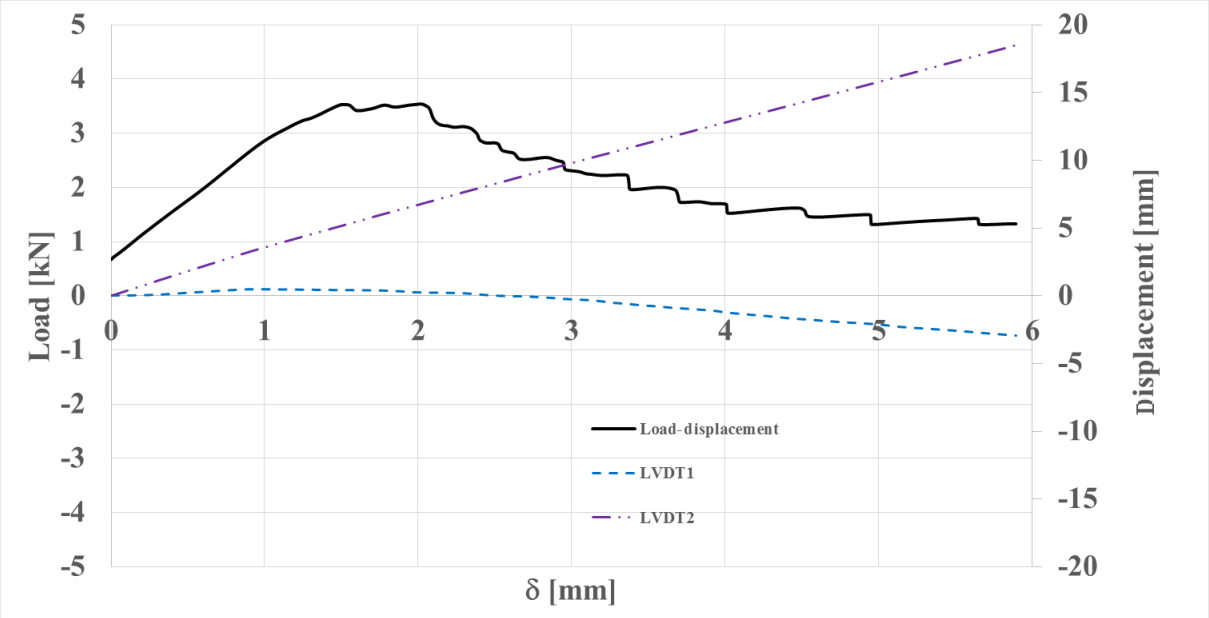

Figure 72: Load- displacement and LVDT's displacement curves for φ=11.25 for dry conditions.

The nominal phase angle is close to pure mode I. This results in some similarities between the *P- δ* curves from pure mode I and mixed mode φ=11.25º.

Using data reduction explained in Section 3.6.3, the resulting R-curves for mode I and mode II are plotted in Figure 73. As expected, the contribution of mode I is more significant than mode

II. For that reason, the R-Curve representing the fracture toughness for mode I is bigger than the R-curve contribution in mode II. The value obtained for mode I was 1.464 N/mm and for mode II was 0.142 N/mm.

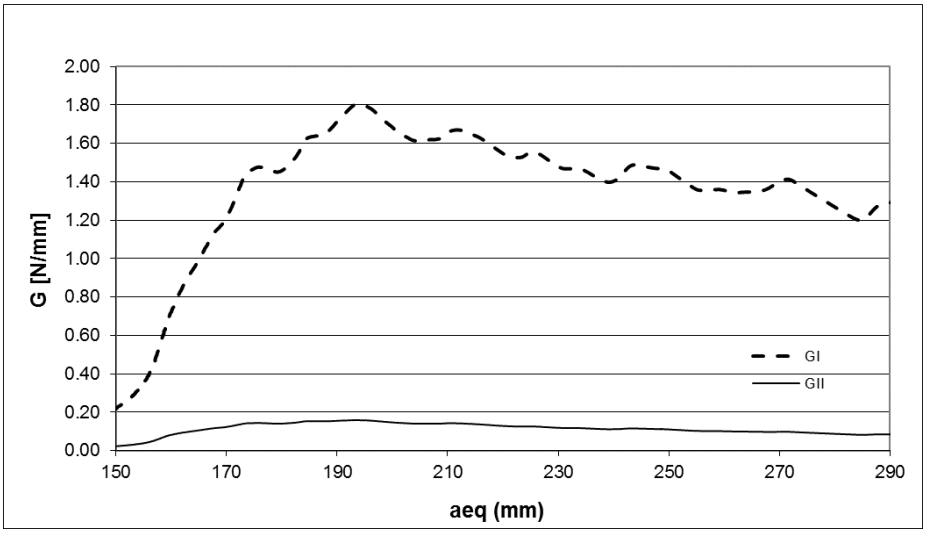

Figure 73: R-curves for mixed mode combination φ=11.25 (dry conditions).

5.4.1.2 Wet

Three tests were performed to obtain the value for fracture toughness in mixed mode combination φ=11.25º under humid conditions. Figure 74 presents the *P*-δ curve and the specimens beams displacements (δ_1 and δ_2) recorded by the LVDTs using a specimen after one month of ageing at 50 ºC. The value of maximum load is close to 3 kN which happens for a displacement of 0.7 mm. This figure presents a decrease in critical load and also a decrease in displacement when compared to dry conditions.

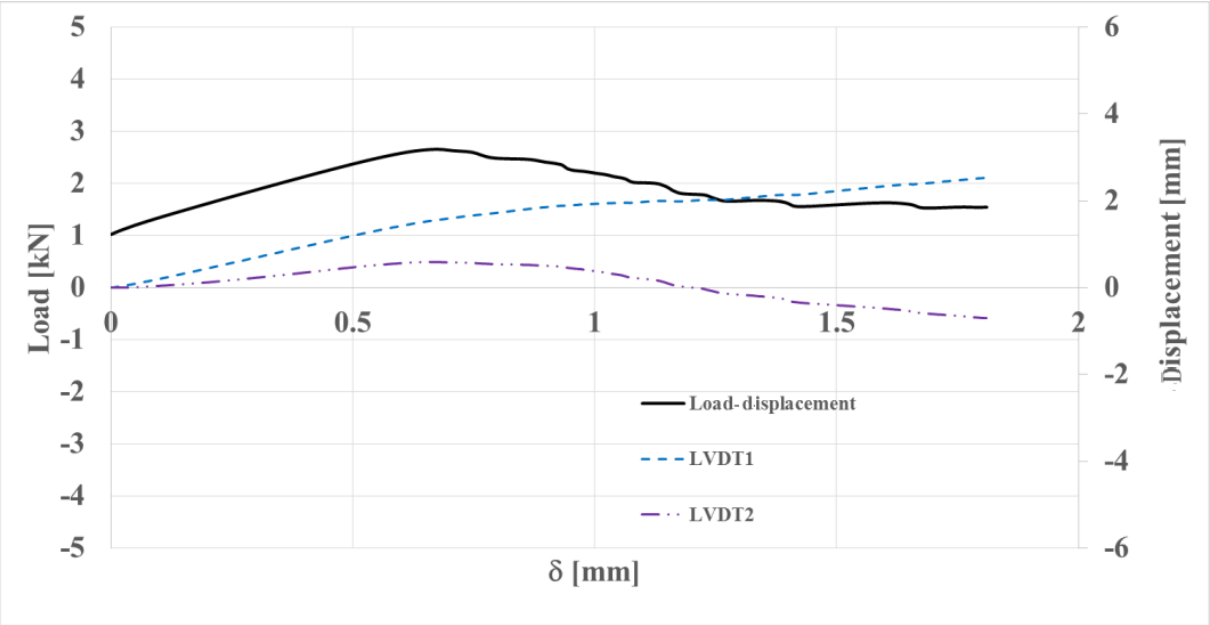

Figure 74: Load- displacement and LVDTs displacement curves for φ=11.25 for wet conditions.

R-curves for mode I and mode II are plotted in Figure 75. The value obtained for mode I was 1.72 N/mm and for mode II was 0.11 N/mm. The total energy, $G_{c,}$ increases from 1.61 to 1.83 N/mm after one month ageing. Wylde and Spelt [31] tested an epoxy system and obtained the same initial increase in wet strength and after 30 days the effect of degradation is visible, as can be seen in Figure 25.

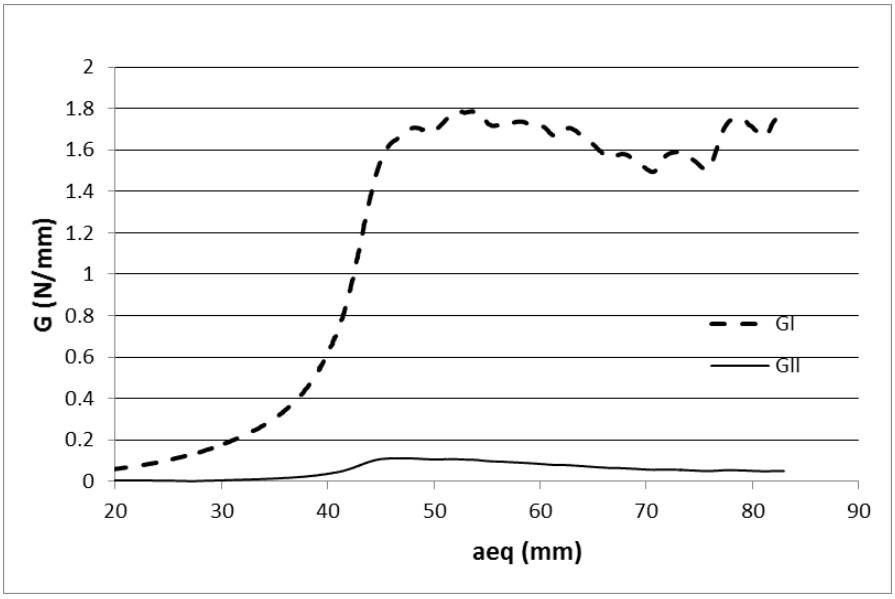

Figure 75: R-curves for mixed mode combination φ=11.25 (wet conditions).

5.4.2 Phase angle: φ= 63º

s_1-s_4 dimensions are described in Table 13 for a phase angle φ=63º. In order to avoid a blunt crack and ensure the crack propagation, the specimens were lightly loaded in mode I before the beginning of the test.

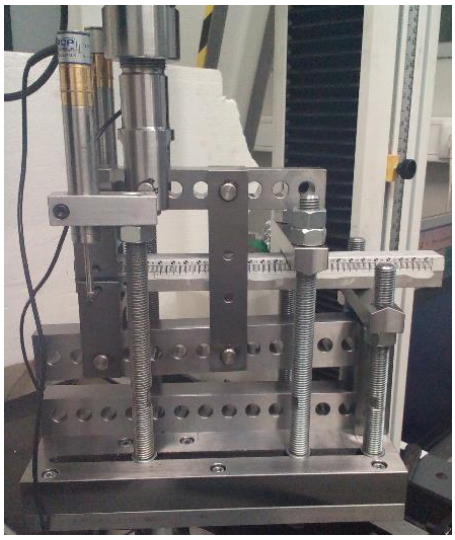

Figure 76: Apparatus with s1-s4 combination for φ=63º.

Table 13: s1-s4 combination for φ=63º.

S1	S2	S3	S4
40	60	100	120

5.4.2.1 Dry

The *P-δ* curve for a phase angle of 63º performed with a dry specimen is shown in Figure 77. The LVDTs displacement is measured and the maximum displacement between beams is 4 mm. The effect of increasing mode II is notorious due to the decreasing in displacement between beams compared to lower phase angles. The *P- δ* curve is more similar to the one from pure mode II than from pure mode I.

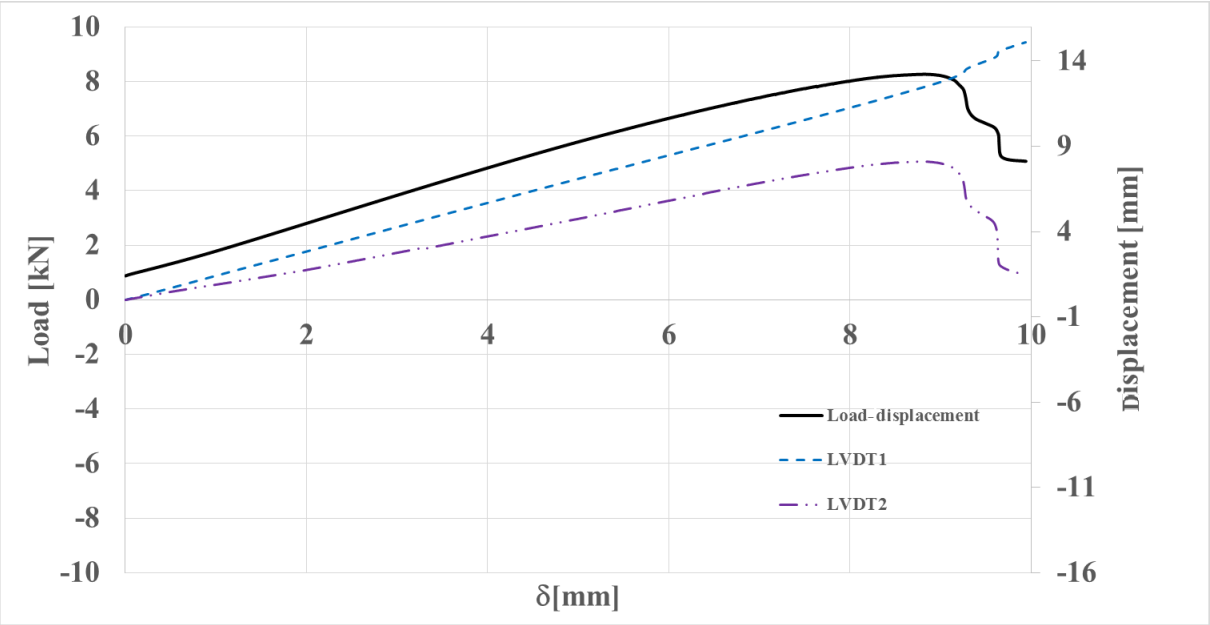

Figure 77: Load- displacement and LVDTs displacement curves for φ=63º for dry conditions.

The R-curves for mode I and mode II are plotted in Figure 78. The values obtained for mode I and mode II were 1.272 N/mm and 5.133 N/mm, respectively. The G_c increases with phase angle, φ. This is the result of the larger fraction of mode II loading.

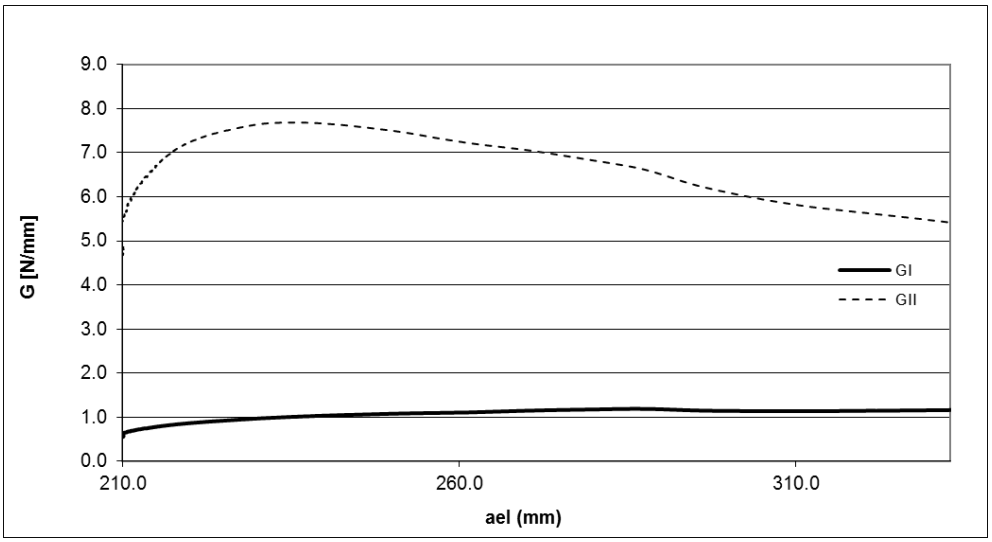

Figure 78: R-curves for mixed mode combination φ=63º (dry conditions).

5.4.2.2 Wet

The *P-δ* curve and the displacements (δ_1 and δ_2) recorded by the LVDT are shown in Figure 79. Comparing Figure 79 with Figure 77, a decrease in the critical load after ageing is verified. The final distance between beams was approximately the same, 4 mm.

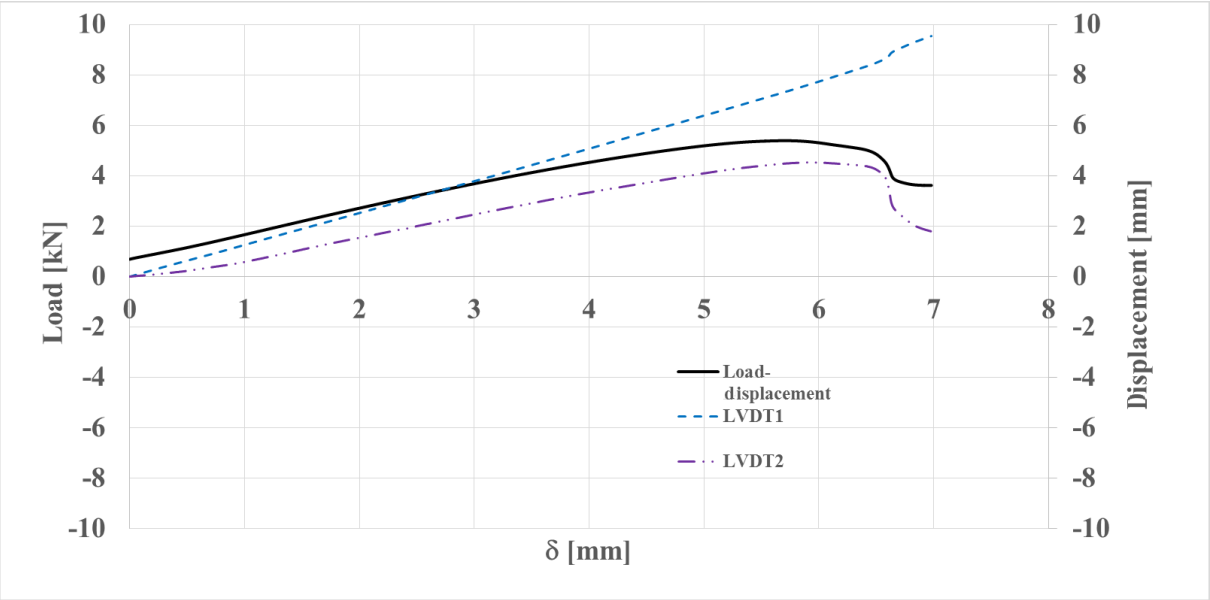

Figure 79: Load- displacement and LVDTs displacement curves for φ=63º for wet conditions.

The R-curves for mode I and mode II are plotted in Figure 80. The value obtained for mode I was 1.47 N/mm and for the mode II component was 4.89 N/mm.

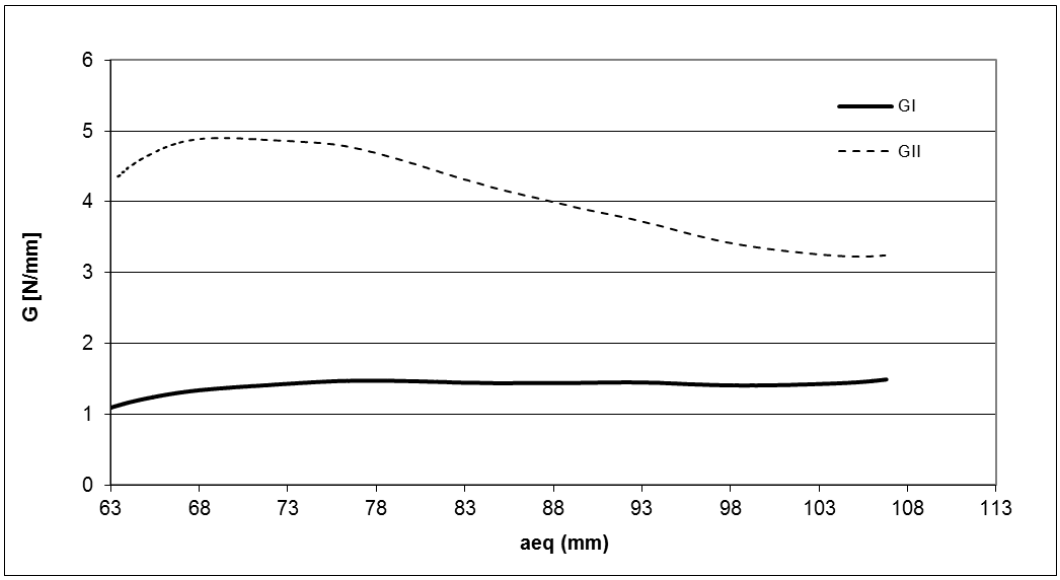

Figure 80: R-curves for mixed mode combination φ=63º (wet conditions).

5.4.3 Phase angle: φ= 77º

The s1-s4 dimensions are described in Table 14 for a phase angle, φ=77º. A pre-crack was done in order to avoid the "blunt" effect.

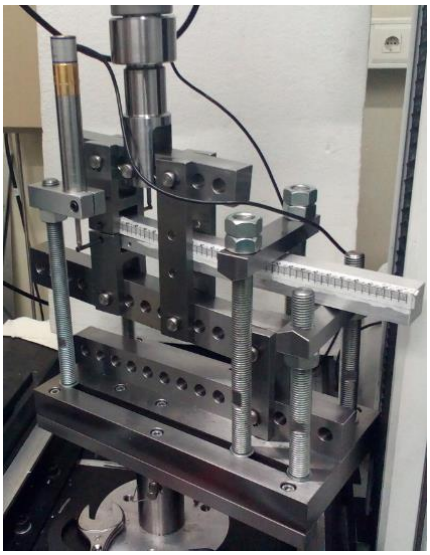

Figure 81: Apparatus with s1-s4 combination for φ=77º.

Table 14: s1-s4 combination for φ=77º.

S1	S2	S3	S4
40	40	80	120

5.4.3.1 Dry

The *P*-δ curve and the displacements (δ_1 and δ_2) recorded by LVDT are shown in Figure 82. A trend is verified for the opening between beams: when the mixed mode combination increases, the distance between δ_1 and δ_2 decreases, showing the proximity to mode II. The distance between substrates is smaller than combinations near mode I, because in this case the loading is close to shear stress.

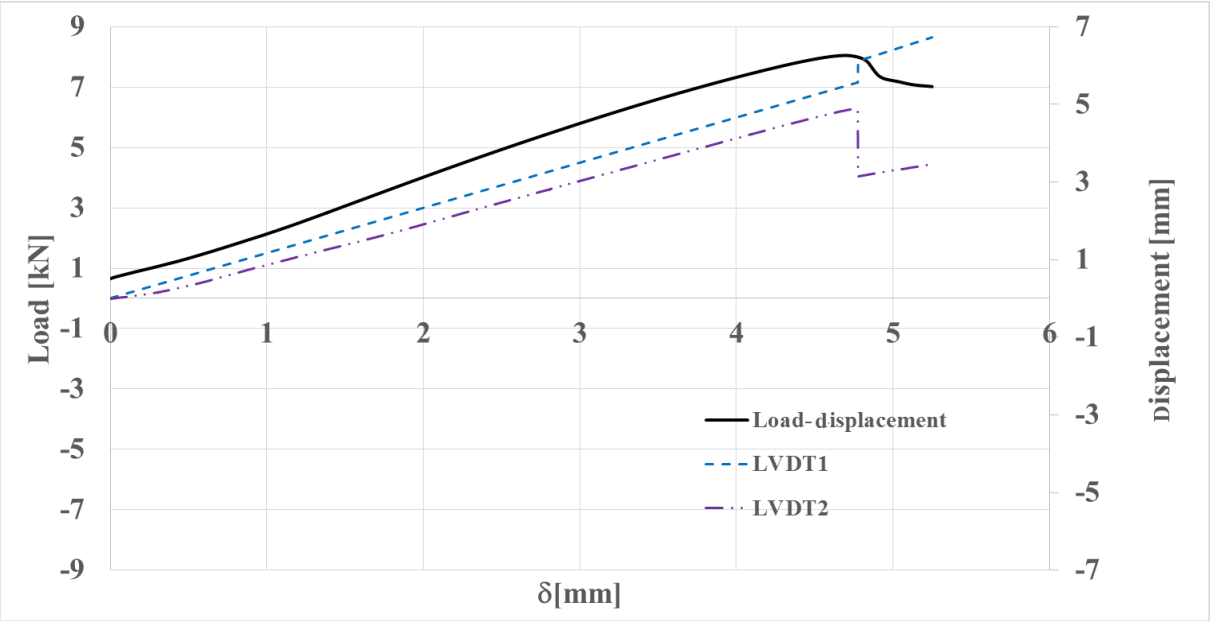

Figure 82: Load- displacement and LVDTs displacement curves for φ=77 for dry conditions.

The R-curves for mode I and mode II are plotted in Figure 83. The values obtained for mode I and mode II were 0.32 N/mm and 8.497 N/mm, respectively. The proximity to mode II presents an increase in total energy release rate.

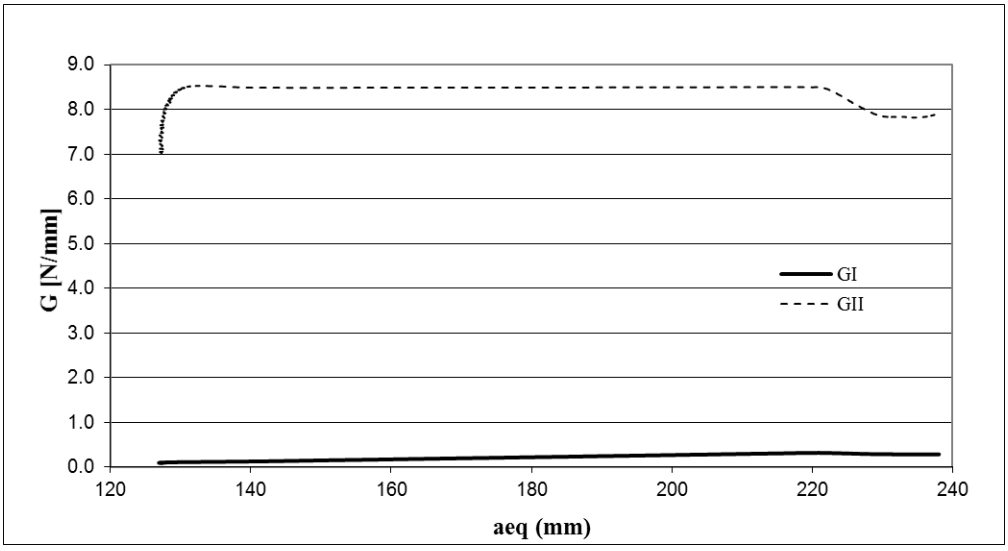

Figure 83: R-curves for mixed mode combination φ=77º (dry conditions).

5.4.3.2 Wet

The *P-δ* curve for a phase angle of 77º performed with a wet specimen is shown in Figure 84. LVDT2 presents some anomalies in values in the first part of test, probably due to some

problems with calibration. However, the final displacement presents a coherent value assuming a distance between beams near to shear stress.

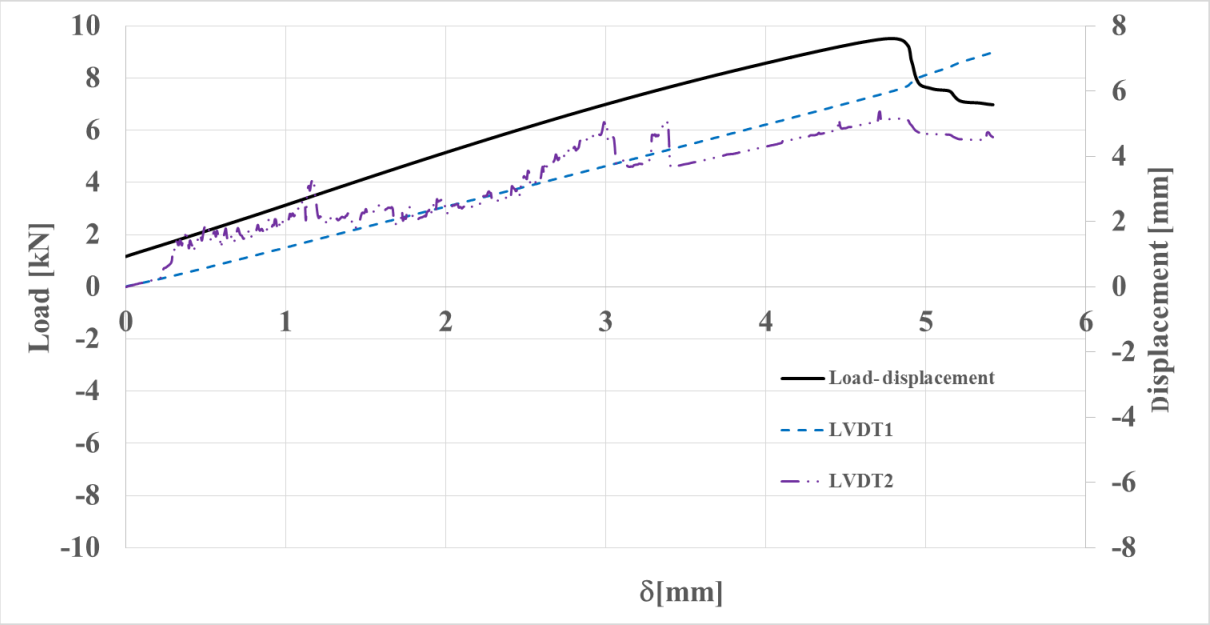

Figure 84: Load- displacement and LVDTs displacement curves for φ=77 for wet conditions.

The R-curves for mode I and mode II are plotted in Figure 85. The values obtained for mode I and mode II were 0.523 N/mm and 8.404 N/mm, respectively.

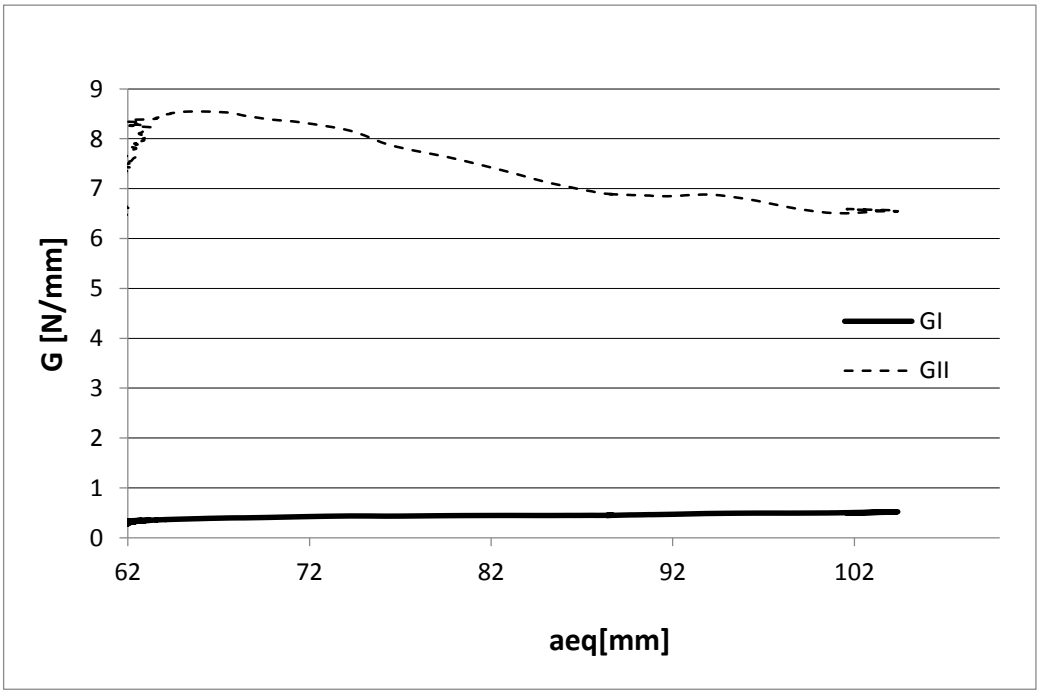

Figure 85: R-curves for mixed mode combination φ=77º (wet conditions).

5.4.4 Mixed-mode analysis

Figure 86 shows the total fracture toughness for a mode combination as a function of energy release rate for mode I of each combination. This shows the effect of the phase angle on degradation. The degraded mixed-mode, G_{cs} values remained proportional to the degraded mode I. This conclusion is in accordance with Ameli et al. [33] as shown in Figure 27, which determines that mixed mode values are proportional to degraded mode I. According to the author, these values are independent of the degradation time and relative humidity.

An increase in the slope for a linear approach is observed. The slopes increase with the phase angles. From Figure 27 the slope phase angle of 27º was 1.29 and with an increasing of mixed mode combination for 48º, the slope increases to 2.13 [33].

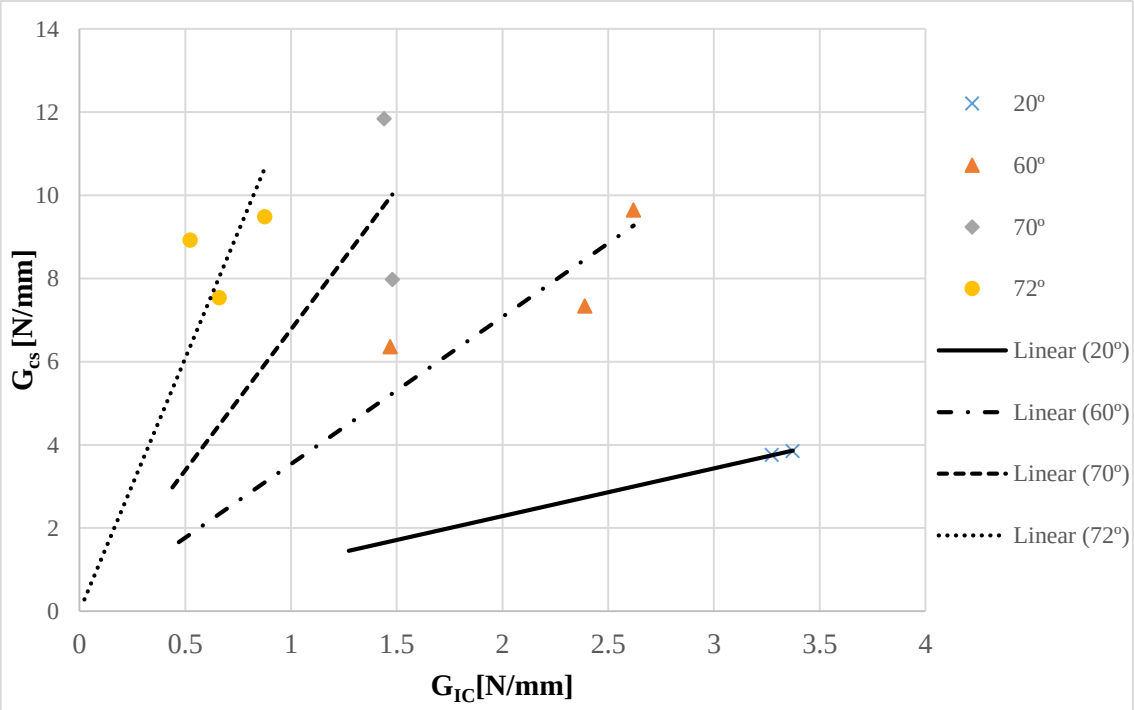

Figure 86: Degraded mixed –mode, G_{cs} values as function of fracture toughness for mode I, G_{IC}.

The mixed mode analysis provides some conclusions:

- In most cases the load has a slight decrease after one month ageing, meaning that when an adhesive joint is under water environments during service life, the load failure is lower than in a dry environment;
- The data provided by the LVDTs is related to the distance between beams and provides some information about which mixed ratio has been studied.

- When the mixed ratio increases, so does the energies release rates, when compared with lower φ values. This happens due to the contribution of the shear stress;

5.5 Fracture envelope analysis for wet and dry conditions

The ultimate strength of an adhesive joint can be predicted using the fracture envelope. This means that the critical energy release rate for mode II, G_{II}, is a function of the fracture toughness for mode I [29, 31].

Figure 87 represents the fracture tests performed, DCB, ENF and mixed-mode for dry specimens and after ageing during one month in distilled water at 50 ºC. All tests were performed using aluminum 7075 as adherend material. It was not verified any plastic deformation. It is noteworthy that different systems were used to perform pure mode and mixed mode.

An increase in fracture toughness was observed for mode I and for almost all the points for mixed mode after ageing. These values are in accordance with literature, which predicts an increase in plasticization [34]. The G_{IC}, in dry conditions, increased from 1.5 N/mm to approximately 3.9 N/mm. The fracture toughness for shear mode is very similar compared to dry specimens. Some reasons can be associated with the value obtained for mode I after ageing:

- When the specimens were placed in distilled water, the blade was not removed. In consequence of that some corrosion was observed in the blade which can lead to anomalies in results;
- The swelling can induce residual stresses in the joint, however during the experimental analysis with bulk specimens (described in Section 3.4.4) did not return any volume variations (after almost one month ageing). For that reason, the swelling was note considered as a plausible explanation to increase the fracture toughness for mode I;
- The use of release agent can influence the properties of the adhesive during the curing. According to McCurdy [47], the use of disbonding agents reduce the fracture toughness for mode I. In fact, the specimens used to test under opening loads did not have release agent, which can explain the severe increase of fracture toughness for mode I;
- According with several authors, the water uptake decreases the T_g [4, 19]. The decreasing of T_g leads to a plasticization of adhesive which can increase the fracture toughness.
- The test of 0.1 mm/min can have an effect on the viscoelasticity of the adhesive.

A linear trend can be observed for both conditions. However, the slope for wet specimens is lower than for dry ones due to the decrease of fracture toughness for mode II. These trend lines represent the maximum values prior to ensure that there will be no crack propagation.

The FTIR analysis and moisture concentration distribution presented in Sections 5.1.1 and 5.1.2 show a qualitative analysis from the water distribution in the adhesive layer. These results provide information about which points present more humidity. According to both analyses, the main conclusion is that water is present in higher quantities in the edges of the DCB specimen.

As mentioned before the water favors the plasticization of the adhesive layer, but in the case of full moisture saturation, the mobility in the chemical structure will be affected [32]. Considering that the specimens used for the ENF test were in distilled water 3 more days than other specimens, some stress relaxation may be associated with a decrease in fracture toughness.

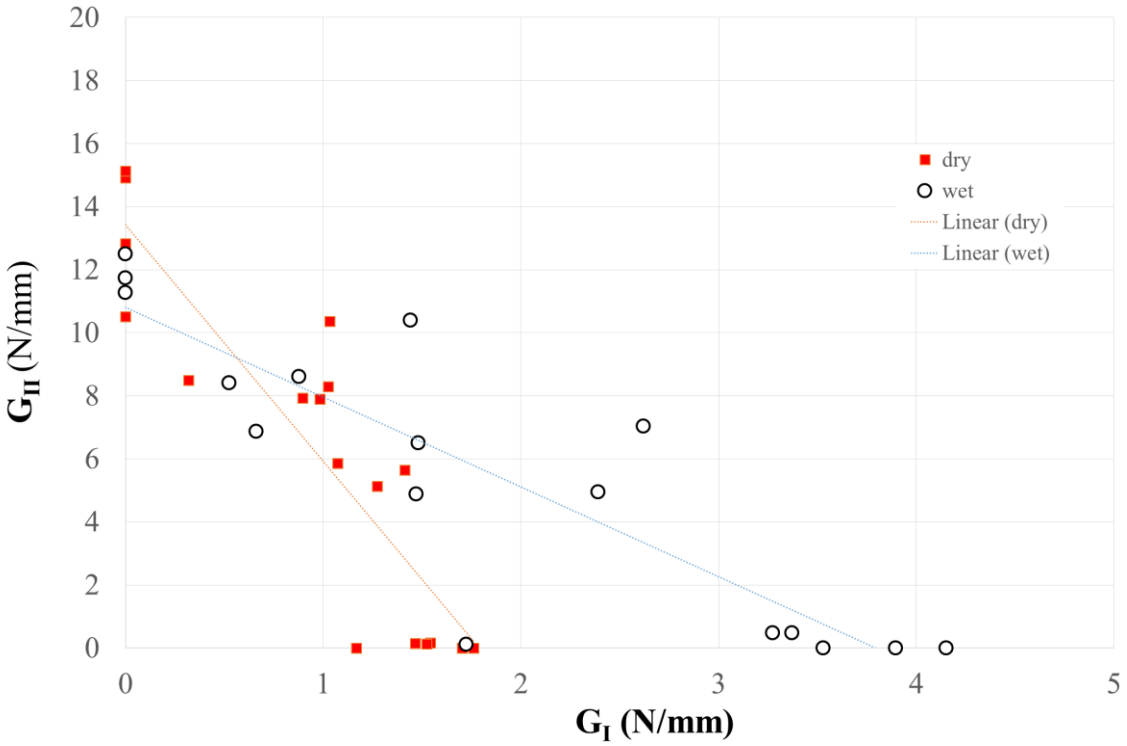

Figure 87: Fracture envelope comparing dry and wet conditions.

6 Conclusions and future works

6.1 Conclusions

This work was a first approach to the effect of ageing in the fracture mechanics properties of aluminium adherends bonded with an epoxy adhesive. Two resulting fracture envelopes for dry and wet conditions were drawn allowing to assess the effect of ageing in the adhesive joint.

The water absorption behaviour of the epoxy adhesive Nagase Chemtex XNR 6852E-2 under complete immersion in water at 50 ºC leads to the following conclusions:

- With water uptake the adhesive presents a dual Fick behaviour;
- For different temperatures, the value of saturation is the same, however the slope in the first Fick is higher for 50 ºC than for 30 ºC;
- FTIR analysis of the functional groups present in both types of samples (dry and wet) shows that there are changes (especially in the –OH group) along the two stages.

The determination of the fracture toughness for the same adhesive (Nagase Chemtex XNR 6852E-2) shows that:

- The fracture toughness for pure and mixed modes of aluminum-epoxy adhesive joints showed a dependence of water uptake by reducing slightly the values for mode II and increasing the values for mode I;
- A decrease on critical loads in load displacement curves for different modes was observed, showing the impact of water uptake;
- Despite the decrease on the critical loads, mode I presented higher displacements resulting in higher values for the energy release rate (G_I), while in mode II the displacements were lower resulting in lower values of energy (G_{II}).
- Using three different and therefore independent setups (pure DCB, ENF, and mixed mode apparatus) allowed to obtain a full fracture envelope with noticeable linear correlation of mode ratios near mode I and mode II to the pure mode I and pure mode II respectively.
- Adding to the complexity of performing mixed-mode I+II tests, the ageing effects on the adhesive bonded joints was an interesting challenge allowing to understand fracture mechanics and chemical properties affecting the adhesive joint behavior, that merits however further study.

6.2 Future works

Some ideas are listed here to improve the results obtained and draw more conclusions:

- Compare different fracture envelopes for different stages of humidity aiming to predict the starting point of adhesive's degradation;
- Select a different temperature for ageing, such as room temperature, to assure the safe design of a structure supported by durability tests;
- Study the irreversible effects in fracture toughness, comparing dry specimens with specimens after desorption with main purpose to understand the influence of corrosion and release agent in the fracture toughness;
- Obtain the stress-strain curve for Nagase Chemtex® XNR 6852E-2 under humid conditions at 50 ºC in order to compare with the values obtained for pure modes;

References

[1] D. M. Banea, "High temperature adhesives for aerospace applications," PhD, Porto, 2011.

[2] L. F. M. d. Silva, A. Öchsner, and R. D. Adams, *Handbook of adhesion technology*: Springer-Verlag, 2011.

[3] Y. C. Lin and X. Chen, "Moisture sorption–desorption–resorption characteristics and its effect on the mechanical behavior of the epoxy system," *Polymer,* vol. 46, pp. 11994-12003, 2005.

[4] A. Q. Barbosa, L. F. M. da Silva, and A. Ochsner, "Hygrothermal aging of an adhesive reinforced with microparticles of cork," *Journal of Adhesion Science and Technology,* vol. 29, pp. 1714-1732, 2015.

[5] F. J. P. Chaves, "Fracture mechanics applied to the design of adhesively bonded joints," PhD, FEUP, Porto, 2013.

[6] R. A. Mata, "Impact of adhesive joints for the automotive industry at low and high temperatures," MsC, IDMEC, University of Porto, 2014.

[7] D. N. Markatos, K. I. Tserpes, E. Rau, S. Markus, B. Ehrhart, and S. Pantelakis, "The effects of manufacturing-induced and in-service related bonding quality reduction on the mode-I fracture toughness of composite bonded joints for aeronautical use," *Composites Part B-Engineering,* vol. 45, pp. 556-564, 2013.

[8] C. V. Katsiropoulos, A. N. Chamos, K. I. Tserpes, and S. G. Pantelakis, "Fracture toughness and shear behavior of composite bonded joints based on a novel aerospace adhesive," *Composites Part B-Engineering,* vol. 43, pp. 240-248, 2012.

[9] N. M. A. Board, *Aerospace Structural Adhesives*: National Academy of Sciences-National Academy of Engineering, 1974.

[10] P. T. de Castro, P. de Matos, P. Moreira, S. Tavares, and V. Ritcher-Trummer, "Problemas de fadiga e fractura em estruturas de aviões fabricadas em alumínio," *Memórias da Academia das Ciências de Lisboa. Lisbon, Portugal,* 2012.

[11] R. D. Adams, *Adhesive Bonding: Science, Technology and Applications*: Elsevier Science, 2005.

[12] Y. Lu, J. Broughton, and P. Winfield, "A review of innovations in disbonding techniques for repair and recycling of automotive vehicles," *International Journal of Adhesion and Adhesives,* vol. 50, pp. 119-127, 2014.

[13] D. News. (15 June). *Automotive Structural Adhesives Drive Material Changes*.

[14] L. F. M. da Silva and C. Sato, *Design of Adhesive Joints Under Humid Conditions*: Springer, 2013.

[15] P. Maxwell James Davis, B.Eng. (Mech), M.Eng. (Mech), RPEQ, A. A. P. L. Director, and A. D. and Andrew McGregor B.Eng (Mech) CPEng, Prosolve Ltd, "<56 Assessing Adhesive Bond Failures - Mixed-Mode Bond Failures Explained.pdf>," *Presented at ISASI Australian Safety Seminar*, 4-6 June 2010 2010.

[16] K. L. D. Daniel O. Adams, Clint Child, "DURABILITY OF ADHESIVELY BONDED JOINTS FOR AIRCRAFT STRUCTURES."

[17] F. J. P. Chaves, L. F. M. da Silva, M. F. S. F. de Moura, D. A. Dillard, and V. H. C. Esteves, "Fracture Mechanics Tests in Adhesively Bonded Joints: A Literature Review," *The Journal of Adhesion,* vol. 90, pp. 955-992, 2013.

[18] V. H. C. Esteves, "Determinação da tenacidade de um adesivo em solicitações de modo misto (I + II)," MsC, 2010.

[19] L. F. M. d. Silva, A. G. d. Magalhães, and M. F. d. S. F. d. Moura, *Juntas adesivas estruturais*. Porto: Publindústria, Edições Técnicas, 2007.

[20] L. F. M. da Silva, D. A. Dillard, B. Blackman, and R. D. Adams, *Testing Adhesive Joints: Best Practices*: Wiley, 2013.

[21] F. J. P. Chaves, M. F. S. F. de Moura, L. F. M. da Silva, and D. A. Dillard, "Numerical validation of a crack equivalent method for mixed-mode I+II fracture characterization of bonded joints," *Engineering Fracture Mechanics,* vol. 107, pp. 38-47, 2013.

[22] Sugiman, "Combined Environmental and Fatigue Degradation of Adhesively Bonded Metal Structures," PhD, Mechanical, Medical and Aerospace Engineering Faculty of Engineering and Physical Sciences, University of Surrey, 2012.

[23] Y. Zhang, R. D. Adams, and L. F. M. da Silva, "Absorption and glass transition temperature of adhesives exposed to water and toluene," *International Journal of Adhesion and Adhesives,* vol. 50, pp. 85-92, 2014.

[24] C.-H. S. G. Springer, "Moisture Absorption and Desorption of Composite Materials," *Journal of Composite Materials 10 (1),* 1976.

[25] W. K. Loh, A. D. Crocombe, M. M. A. Wahab, and I. A. Ashcroft, "Modelling anomalous moisture uptake, swelling and thermal characteristics of a rubber toughened epoxy adhesive," *International Journal of Adhesion and Adhesives,* vol. 25, pp. 1-12, 2005.

[26] G. Z. Xiao and M. E. R. Shanahan, "Swelling of DGEBA/DDA epoxy resin during hygrothermal ageing," *Polymer,* vol. 39, pp. 3253-3260, 1998.

[27] C. D. M. Liljedahl, A. D. Crocombe, F. E. Gauntlett, M. S. Rihawy, and A. S. Clough, "Characterising moisture ingress in adhesively bonded joints using nuclear reaction analysis," *International Journal of Adhesion and Adhesives,* vol. 29, pp. 356-360, 2009.

[28] D. D. A. Bond, "The effect of environmental moisture on the performance and certification of adhesively bonded joints & repairs," in *FAA & CAA Workshop on Bonded Structures*, University of Manchester UK, 2004.

[29] A. Ameli, N. V. Datla, S. Azari, M. Papini, and J. K. Spelt, "Prediction of environmental degradation of closed adhesive joints using data from open-faced specimens," *Composite Structures,* vol. 94, pp. 779-786, 2012.

[30] W. K. Loh, A. D. Crocombe, M. M. A. Wahab, and I. A. Ashcroft, "Environmental degradation of the interfacial fracture energy in an adhesively bonded joint," *Engineering Fracture Mechanics,* vol. 69, pp. 2113-2128, 2002.

[31] J. W. Wylde and J. K. Spelt, "Measurement of adhesive joint fracture properties as a function of environmental degradation," *International Journal of Adhesion and Adhesives,* vol. 18, pp. 237-246, 1998.

[32] G. LaPlante and P. Lee-Sullivan, "Moisture effects on FM300 structural film adhesive: Stress relaxation, fracture toughness, and dynamic mechanical analysis," *Journal of Applied Polymer Science,* vol. 95, pp. 1285-1294, 2005.

[33] A. Ameli, M. Papini, and J. K. Spelt, "Fracture R-curve of a toughened epoxy adhesive as a function of irreversible degradation," *Materials Science and Engineering a-Structural Materials Properties Microstructure and Processing,* vol. 527, pp. 5105-5114, 2010.

[34] A. Ameli, N. V. Datla, M. Papini, and J. K. Spelt, "Hygrothermal Properties of Highly Toughened Epoxy Adhesives," *Journal of Adhesion,* vol. 86, pp. 698-725, 2010.

[35] Z. C. Li, D. Hayward, R. Gilmore, and R. A. Pethrick, "Investigation of moisture ingress into adhesive bonded structures using high frequency dielectric analysis," *Journal of Materials Science,* vol. 32, pp. 879-886, 1997.

[36] A. J. Kinloch, *Adhesion and Adhesives: Science and Technology*: Springer, 1987.

[37] C. M. S. Canto, "Strength and fracture energy of adhesives for the automotive industry," MsC, FEUP, Porto, 2013.

[38] G. M. S. d. O. Viana, "Functionally graded adhesive patch repairs in civil applications," MsC, FEUP, Porto, 2013.

[39] *ISO 294-3: Plastics - Injection Moulding of Test Specimens of Thermoplastic Materials - Part 3 :Plaques de Petites Dimensions*: ISO, 2002.

[40] D. F. S. Saldanha, C. Canto, L. F. M. da Silva, R. J. C. Carbas, F. J. P. Chaves, K. Nomura, *et al.*, "Mechanical characterization of a high elongation and high toughness epoxy adhesive," *International Journal of Adhesion and Adhesives,* vol. 47, pp. 91-98, 2013.

[41] A. Mubashar, I. A. Ashcroft, G. W. Critchlow, and A. D. Crocombe, "Modelling Cyclic Moisture Uptake in an Epoxy Adhesive," *Journal of Adhesion,* vol. 85, pp. 711-735, 2009.

[42] M. F. S. F. de Moura, "Numerical simulation of the ENF test for the mode-II fracture characterization of bonded joints," *Journal of Adhesion Science and Technology,* vol. 20, pp. 37-52, 2006.

[43] R. D. S. G. Campilho, "Repair of composite and wood structures," PhD, Porto, 2009.

[44] Y. Diamant, G. Marom, and L. J. Broutman, "The effect of network structure on moisture absorption of epoxy resins," *Journal of Applied Polymer Science,* vol. 26, pp. 3015-3025, 1981.

[45] G. Z. Xiao and M. E. R. Shanahan, "Irreversible effects of hygrothermal aging on DGEBA/DDA epoxy resin," *Journal of Applied Polymer Science,* vol. 69, pp. 363-369, 1998.

[46] F. G. A. Silva, J. J. L. Morais, N. Dourado, J. Xavier, F. A. M. Pereira, and M. F. S. F. de Moura, "Determination of cohesive laws in wood bonded joints under mode II loading using the ENF test," *International Journal of Adhesion and Adhesives,* vol. 51, pp. 54-61, 2014.

[47] R. H. McCurdy, A. R. Hutchinson, and P. H. Winfield, "The mechanical performance of adhesive joints containing active disbonding agents," *International Journal of Adhesion and Adhesives,* vol. 46, pp. 100-113, 2013.

Appendix A: Fracture tests results

Fracture envelope for Nagase XNR 6852E -2 (dry)

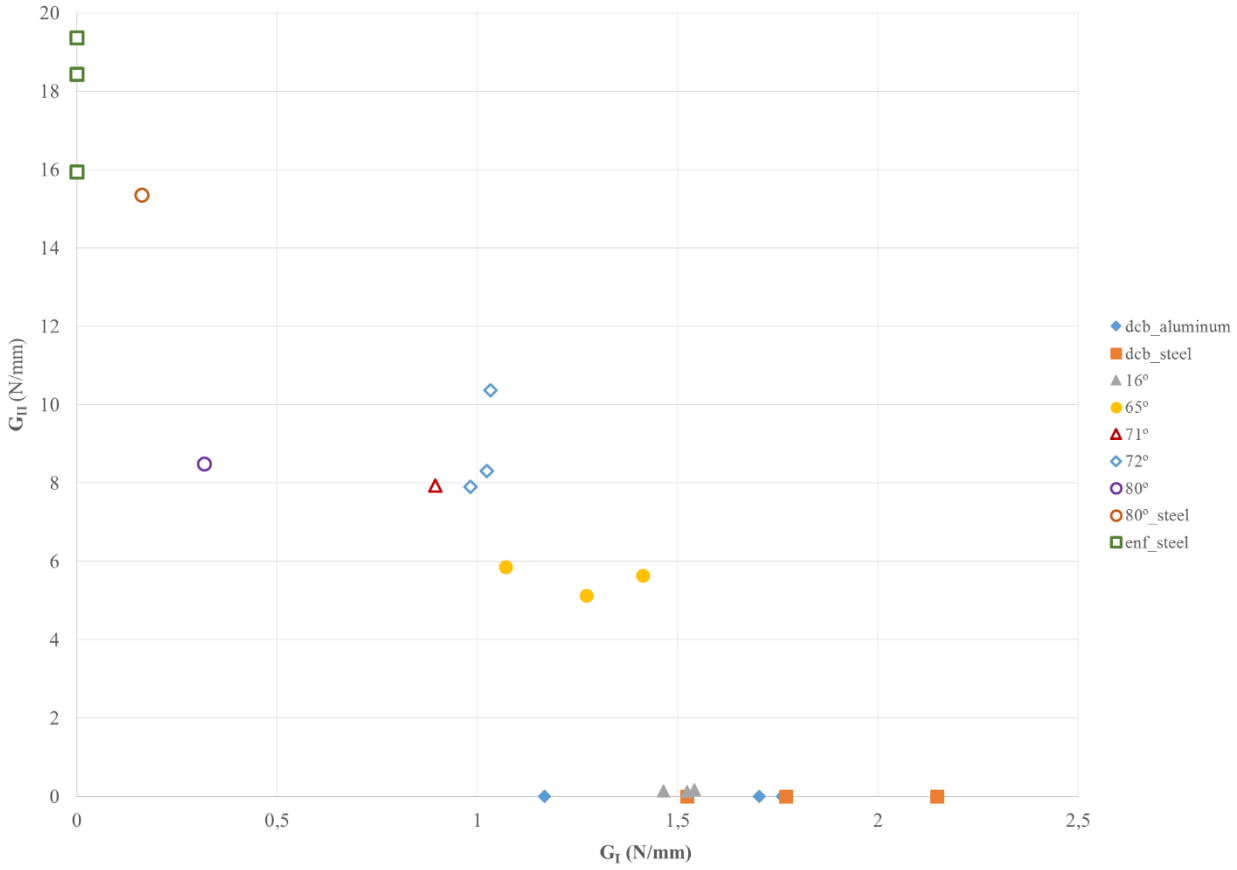

Appendix B: FTIR

FTIR analysis in 12 points over adhesive layer.